Journal of Research of the National Bureau of Standards Vol. 60, No. 5, May 1958 Research Paper 2857

Forces on Cylinders and Plates in an Oscillating Fluid [1]

Garbis H. Keulegan and Lloyd H. Carpenter

The inertia and drag coefficients of cylinders and plates in simple sinusoidal currents are investigated. The midsection of a rectangular basin with standing waves surging in it is selected as the locale of currents. The cylinders and plates are fixed horizontally and below the water surface. The average values of the inertia and drag coefficients over a wave cycle show variations when the intensity of the current and the size of the cylinders or plates are changed. These variations, however, can be correlated with the period parameter U_mT/D, where U_m is the maximum intensity of the sinusoidal current, T is the period of the wave and D is the diameter of the cylinder or the width of the plate. For the cylinders U_mT/D equaling 15 is a critical condition yielding the lowest value of the inertia coefficient and the largest value of the drag coefficient. For the plates the higher values of the drag coefficient are associated with the smaller values of U_mT/D and the higher values of the mass coefficient with the larger values of U_mT/D. The variation of the coefficients with the phase of the wave is examined and the bearing of this on the formula for the forces is discussed. The flow patterns around the cylinders and plates are examined photographically, and a suggestion is advanced as to the physical meaning of the parameter U_mT/D.

1. Introduction

In a remarkable paper on the motion of pendulums Stokes showed that the expression for the force on a sphere oscillating in an unlimited viscous fluid consists of two terms, one involving the acceleration of the sphere and the other the velocity [1].[2] Furthermore, the inertia coefficient involved in the acceleration term is modified because of viscosity and, indeed, is augmented over the theoretical value valid for irrotational flow. The drag coefficient associated with the velocity term is modified because of the acceleration, and its value is greater than it would be if the sphere were moving with a constant velocity. Subsequent to Stokes' studies, the forces on a sphere moving in a viscous fluid in an arbitrary manner were investigated by Boussinesq and also by Basset [2, 3]. They found that the force experienced by a sphere at a given time depends, in general, on the entire history of its acceleration as well as the instantaneous velocity and acceleration. As an example, if a sphere is accelerated, say with a constant acceleration, from a position of rest to a finite velocity and is then kept at this velocity, the force during the initial instants of uniform velocity differs from the force occurring at a later time. Rayleigh has given the formula for the force for this case [4]. The force expression of Boussinesq-Basset contains three terms, one of which is in the form of an integral involving the history of acceleration. If the integral is evaluated when the acceleration is represented by a sinusoidal function it then yields the modifications of the inertia and drag coefficients in Stokes' formula.

One expects quantitatively different results when the oscillating velocities are large and the flow turbulent. As yet a theoretical analysis of the problem is difficult and much of the desired information must be obtained experimentally. In this respect the experimental studies have been dealt with variously. One method is due to McNown and Wolf [5], who considered the force on a two-dimensional object immersed in a flow as made up of three parts:

$$F=A_0\rho\frac{d(kU)}{dt}+\oint p_x dS+\frac{1}{2}C_dD\rho U|U|, \qquad (1)$$

where F is the force per unit length in the direction of flow, x; U the velocity at points far removed from the object; p_x, the x-component of the ambient pressure in the absence of the body; dS, an element of the surface area; C_d, the coefficient of drag; and k, the virtual mass coefficient. The dimension of the body normal to the flow is D, and A_0 is a circular area, $A_0=\pi D^2/4$, to which the added mass is referred. If A is the cross-sectional area of the body, $A=rA_0$, r being a ratio, then

$$\oint p_x dS=\rho rA_0\frac{dU}{dt},$$

and finally

$$F=A_0\rho\left[\frac{d(kU)}{dt}+r\frac{dU}{dt}\right]+\frac{1}{2}C_dD\rho U|U|.$$

In this approach the variability of the mass coefficient, k, is implied. Thus, introducing a new coefficient k' such that

$$k'\frac{dU}{dt}=\frac{d}{dt}(kU)$$

and putting

$$C_m=(k'+r), \qquad (3)$$

there is obtained from eq (1), the expression

$$F=C_m\rho A_0\frac{dU}{dt}+\frac{1}{2}C_dD\rho U|U|, \qquad (4)$$

which in fact constitutes a second approach utilized first by Morison and coinvestigators [6, 7]. The form of the expression is in agreement with the Stokes formula for force on a sphere oscillating in a viscous medium. In a general sense one may still regard C_m as a kind of mass or inertia coefficient.

[1] Investigation sponsored by the Office of Naval Research.
[2] Figures in brackets indicate the literature references at the end of this paper.

A third approach was proposed by Iversen and Balent, who considered the force on an accelerated disk moving in one direction [8]. Briefly,

$$F=C\rho DU^2, \tag{5}$$

where

$$C=C\left(\frac{DU}{\nu}, \frac{D}{U^2}\frac{dU}{dt}\right).$$

Keim has considered the case of accelerated cylinders [9] and Bugliarello that of accelerated spheres [10], all motions being in one direction. Here the resort is to a single coefficient C and attempts to separate the effects of acceleration and viscosity have not been shown to be successful. Accordingly, the adoption of this method can have a meaning only for monotonic motions subject to definite limitations as to initial and final conditions.

For oscillatory motions, although the forces are more accurately described either using eq (2) or eq (4), the latter might be preferred provided the coefficients C_m and C_d could be predicted with some precision. The application of the expression to vertical piling and large submerged objects by Reid and Bretschneider stresses the necessity of having these coefficients better determined [11].

On the basis of irrotational flow around the cylinder, C_m should equal 2, and one may suppose that the value of C_d should be identical with that applicable to a constant velocity. Morison and coinvestigators have obtained the values of C_d and C_m in particular cases by considering the observed forces in the phases of the wave cycle where U or dU/dt vanishes. Such determinations show considerable variations of C_m from the theoretical value and of C_d from the steady state value at the corresponding Reynolds number. Dealing with field studies at Caplen, Texas, R. O. Reid found similar variations in C_m and C_d [12]. The variations in the coefficients, however, have not yet been correlated with any appropriate parameter.

The present investigation was undertaken with the following two objectives in mind. The first was in regard to a supplementary function ΔR that could be introduced in eq (4) for a truer representation of force when considering the coefficients C_m and C_d as being constant throughout a given wave cycle. The necessity for the term ΔR is associated with the eventuality that the point values of C_m and C_d deviate from their average values. The second objective was to examine the possibility of correlating the average values of C_m and C_d with a parameter U_mT/D, where U_m is the amplitude of the harmonically varying velocity, T is the period of the oscillations, and D is the diameter of a cylinder or the breadth of a rectangular plate. The mid-cross section of a large rectangular vessel with standing waves surging in it was chosen as the field of harmonically varying current. The cylinders and plates were held fixed horizontally, totally submerged in water and extending from one side of the vessel to the other to approximate as closely as possible the condition of infinite length.

2. Fluid Forces on an Immersed Body at Rest in a Moving Liquid

It would be instructive to consider the momentum equations discussed by Murnaghan for the evaluation of force on objects immersed in a perfect liquid [13]. The method, however, is now generalized to apply to imperfect liquids.

Consider the case of two-dimensional flow with x horizontal and z vertical. The equation of motion in the x-direction is

$$\rho\left(\frac{\partial u}{\partial t}+u\frac{\partial u}{\partial x}+w\frac{\partial u}{\partial z}\right)=\frac{\partial p_{xx}}{\partial x}+\frac{\partial p_{zx}}{\partial z}, \tag{6}$$

where u and w are the velocity components along the axes x and z, ρ the density of the liquid, p_{xx} the normal stress on an elementary surface perpendicular to x, and p_{zx} the tangential stress on an elementary surface normal to z, the stress being in the direction of x. Because of the incompressibility of the liquid,

$$\frac{\partial u}{\partial x}+\frac{\partial w}{\partial z}=0 \tag{7}$$

and eq (2) becomes

$$\rho\frac{\partial u}{\partial t}+\rho\left(\frac{\partial}{\partial x}u^2+\frac{\partial}{\partial z}uw\right)=\frac{\partial p_{xx}}{\partial x}+\frac{\partial p_{zx}}{\partial x}. \tag{8}$$

Take the immersed cylindrical body of surface S, as in figure 1, and draw a surface S' of arbitrary shape which encloses the cylinder. Let ω be the region bounded by S and S' and l and n the direction cosines of the normal drawn inward into the region. Integrating eq (8) throughout ω, and in this making use of Green's Theorem, one finds

$$\rho\int\frac{\partial u}{\partial t}d\omega-\rho\int u(lu+nw)dS-\rho\int u(lu+nw)dS'=$$
$$-\int(lp_{xx}+np_{zx})dS-\int(lp_{xx}+np_{zx})dS'. \tag{9}$$

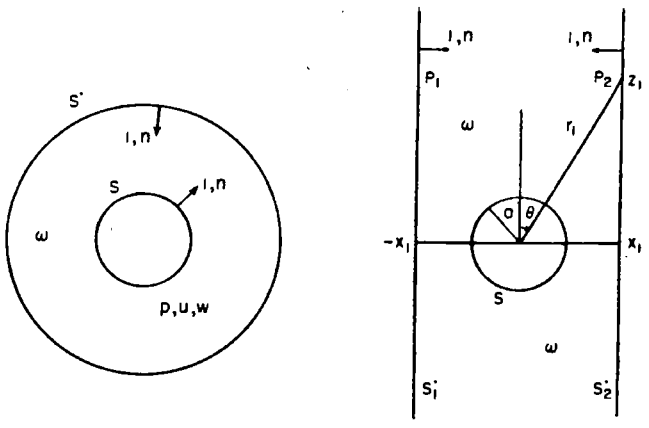

FIGURE 1. *Notation diagram for force analysis.*

Over the surface S of the immersed body $lu+nw$ vanishes because the body is at rest. Also $\int(lp_{xx}+np_{xz})dS=F$, that is, the x-component of the force exerted on the solid by the moving liquid. It may be assumed that if S' is removed sufficiently from the body the tangential stress p_{xz} on S' vanishes and the normal stress p_{xx} reduces to the hydrostatic pressure $-p$. Solving for F,

$$F=-\rho\int\frac{\partial u}{\partial t}d\omega+\rho\int u(lu+nw)dS'+\int lpdS'. \quad (10)$$

The later relation may be given in another form, suitable for the present purpose. Select the bounding surface S' as the rectangular strip shown in figure 1. The plane S_1' to the left of the cylinder passes through the point $x=-x_1$ and the plane S_2' to the right passes through $x=x_1$. Denoting the horizontal velocity components at the points P_1 and P_2 with the common elevation z_1 by u_1 and u_2, and the pressures by p_1 and p_2, eq (10) now reduces to

$$F=-\rho\int_\omega\frac{\partial u}{\partial t}d\omega+\rho\int_{-\infty}^{+\infty}(u_1^2-u_2^2)dz_1+\int_{-\infty}^{+\infty}(p_1-p_2)dz_1, \quad (11)$$

which is the momentum equation of familiar form.

This may be specialized to evaluate the force on a circular cylinder when the motion is irrotational. Letting U be the undisturbed velocity and referring to Lamb [14],

$$\left.\begin{aligned} u&=U\left[1+\frac{a^2}{r^2}\cos 2\theta\right]\\ w&=-U\frac{a^2}{r^2}\sin 2\theta\\ \frac{p}{\rho}&=\frac{dU}{dt}\left(r+\frac{a^2}{r}\right)\sin\theta-\frac{1}{2}(u^2+w^2)\end{aligned}\right\}, \quad (12)$$

where a is the radius of the cylinder, r is radial distance, and θ is the angle between a radius vector and the vertical line $x=0$ passing through the center of the cylinder. Clearly, $u_1=u_2$ and the momentum equation, eq (11), reduces to

$$F_1=-\rho\int_\omega\frac{\partial u}{\partial t}d\omega+\int_{-\infty}^{\infty}(p_1-p_2)dz_1. \quad (13)$$

Introducing the values of u and p from eq (12), and omitting the straightforward but somewhat lengthy evaluations, the result is

$$F_1=2\pi\frac{dU}{dt}a^2\rho,$$

or in terms of the diameter D of the cylinder

$$F_1=C_m\frac{\rho\pi D^2}{4}\frac{dU}{dt}, \quad (14)$$

where $C_m=2$.

Next, suppose that the undisturbed velocity is constant and that the body experiences a drag. With the liquid extending to infinity and ignoring the variation of pressures from the shedding eddies, or, more properly, assuming that the surfaces S_1' and S_2' are far removed from the cylinder, $p_1=p_2$, and eq (11) reduces to

$$F_2=\rho\int_{-\infty}^{+\infty}(u_1^2-u_2^2)dz_1. \quad (15)$$

The velocity $u_1=U$, and $u_2=mU$, where m is dependent on z_1/D and on Reynolds number UD/ν. Thus,

$$F_2=C_d\rho D\frac{U^2}{2} \quad (16)$$

where

$$C_d=2\int_{-\infty}^{+\infty}(1-m^2)d\frac{z_1}{D}.$$

It appears that in ordinary cases where the flow departs from irrotationality and becomes unsteady and eddying, eq (11) is still the basis for evaluating the force, since the first and third integrals may be associated with acceleration and the second with drag. That is, the coefficients C_m and C_d are derived from eq (13) and (15) provided the velocities and pressures can be given. The force of the statement is only academic, since in the flows involving separation and intermittent eddy formation the pressures and velocities are not known and the integrations in eq (11), at present, cannot be carried out. Nevertheless, experience suggests that eq (4) remains useful at least for sinusoidal motions, if allowance can be made for the variations in C_m and C_d.

Had one carried out the integrations in eq (11) for an extended plate using the known velocity expressions derived from the Kirchoff solution for the impact on a lamina, definite values for C_m and C_d would have resulted. This would have shown in principle the existence of a relation between C_m and C_d in the absence of eddy formation. In the Kirchoff solution the wake is of infinite length and this is cause for concern. McNown overcomes this difficulty by considering the case of a closed wake as between two plates and finds a relation between k and C_d or between C_m and C_d [15]. This result is very significant as it points to the path to be followed in analytical approaches taking into account also the effect of the eddy processes. With cylinders the changing separation seats are a cause of added difficulty.

Meanwhile, the tasks of the experimental investigations become more necessary. Not only are the needs of the applied arts to be fulfilled, but also there must be clarification as regards the flow processes during unsteady flows.

3. Cylinder in a Field of Sinusoidal Motion

Forces on a cylinder admit an easier representation when the undisturbed portion of the flow, infinite in extent, is varying harmonically. Let the velocity be given by

$$U=-U_m \cos \sigma t, \tag{17}$$

where U_m is the semiamplitude of the current, T the period of the alternations, and $\sigma=2\pi/T$. The force on the cylinder per unit length F is in general

$$F=f(t,T,U_m,D,\rho,\nu). \tag{18}$$

Grouping the variables on the basis of dimensional reasoning

$$\frac{F}{\rho U_m^2 D}=f\left(\frac{t}{T}, \frac{U_m T}{D}, \frac{U_m D}{\nu}\right),$$

or introducing

$$\theta=2\pi t/T, \quad = \omega t \tag{19}$$

$$\frac{F}{\rho U_m^2 D}=f\left(\theta, \frac{U_m T}{D}, \frac{U_m D}{\nu}\right), \tag{20}$$

where $U_m D/\nu$ is a Reynolds number and $U_m T/D$ will be termed the "period parameter." Bearing in mind that F is periodic, and that because of flow symmetry

$$F(\theta)=-F(\theta+\pi),$$

we have

$$\frac{F}{\rho U_m^2 D}=A_1 \sin \theta+A_3 \sin 3\theta+A_5 \sin 5\theta+\ldots$$
$$+B_1 \cos \theta+B_3 \cos 3\theta+B_5 \cos 5\theta+\ldots. \tag{21}$$

Here the coefficients $A_1, A_3 \ldots$, and $B_1, B_3 \ldots$ are independent of θ, and are at most functions of $U_m T/D$ and $U_m D/\nu$. A sure method of approach in the analysis of the observed force curve is to resort to a Fourier analysis to determine the coefficients $A_1 \ldots B_1 \ldots$.

$$A_n=\frac{1}{\pi}\int_0^{2\pi} \frac{F \sin n\theta}{\rho U_m^2 D}\, d\theta \tag{22}$$

and

$$B_n=\frac{1}{\pi}\int_0^{2\pi} \frac{F \cos n\theta}{\rho U_m^2 D}\, d\theta. \tag{23}$$

Once the coefficients are obtained, their dependence on $U_m T/D$ and $U_m D/\nu$ may be established, provided the observational data are of sufficient number and of large extent.

The above general and fundamental relation, eq (21), may be reconciled with eq (4), which is the form which Morison and coinvestigators Reid, Bretschneider and others, have adopted in their numerous studies. Introducing U from eq (17) into eq (4)

$$\frac{F}{\rho U_m^2 D}=\frac{\pi}{4} C_m \cdot \frac{D\sigma}{U_m} \sin \theta-\frac{C_d}{2} |\cos \theta| \cos \theta. \tag{24}$$

By the rule of Fourier

$$|\cos \theta| \cos \theta=\sum_{n=0}^{\infty} \frac{\int_0^{2\pi} |\cos \theta| \cos \theta \cos n\theta\, d\theta}{\int_0^{2\pi} \cos^2 n\theta\, d\theta}$$
$$=a_0+a_1 \cos \theta+a_2 \cos 2\theta+a_3 \cos 3\theta+\ldots,$$

where

$$a_n=0 \text{ for } n \text{ even},$$

$$a_n=(-1)^{\frac{n+1}{2}} \frac{8}{n(n^2-4)\pi} \text{ for } n \text{ odd},$$

$$a_1=\frac{8}{3\pi}, \; a_3=\frac{8}{15\pi}, \; a_5=-\frac{8}{105\pi}, \ldots. \tag{25}$$

Introducing this in eq (21), and writing

$$\left.\begin{aligned} B_1'&=\frac{B_1}{a_1} \\ B_3'&=B_3-\frac{a_3}{a_1} B_1 \\ B_5'&=B_5-\frac{a_5}{a_1} B_1 \end{aligned}\right\} \tag{26}$$

one has

$$\frac{F}{\rho U_m^2 D}=A_1 \sin \theta+A_3 \sin 3\theta+A_5 \sin 5\theta+\ldots$$
$$+B_1' |\cos \theta| \cos \theta+B_3' \cos 3\theta+B_5' \cos 5\theta+\ldots. \tag{27}$$

Now eq (24) and (27) may be compared. One can write

$$\frac{\pi}{4} C_m \cdot \frac{D\sigma}{U_m}=A_1+A_3 \frac{\sin 3\theta}{\sin \theta}+A_5 \frac{\sin 5\theta}{\sin \theta}\ldots$$

and

$$\frac{C_d}{2}=-B_1'-B_3' \frac{\cos 3\theta}{|\cos \theta| \cos \theta}-\frac{B_5' \cos 5\theta}{|\cos \theta| \cos \theta}+\ldots,$$

or

$$C_m(\theta)=\frac{2}{\pi^2} \frac{U_m T}{D} [A_1+A_3+A_5+2(A_3$$
$$+A_5) \cos 2\theta+2A_5 \cos 4\theta+\ldots] \tag{28}$$

and

$$C_d(\theta)=-2B_1'+\frac{2}{|\cos \theta|} [2(B_3'-B_5')+4(B_5'-B_3') \cos 2\theta$$
$$-4B_5' \cos 4\theta+\ldots]. \tag{29}$$

Thus if A_3, A_5, and B_3', B_5' vanish, the coefficients of mass and drag remain constant for all the phases

in the wave cycle and

$$C_m=\frac{2}{\pi^2}\frac{U_mT}{D}A_1=\frac{2}{\pi^3}\frac{U_mT}{D}\int_0^{2\pi}\frac{F\sin\theta d\theta}{\rho U_m^2D} \tag{30}$$

and

$$C_d=-2B_1'=-\frac{3}{4}\int_0^{2\pi}\frac{F\cos\theta d\theta}{\rho U_m^2D}. \tag{31}$$

In the event that these coefficients vary with the phase θ of the wave cycle, the values given by eq (30) and (31) are in a sense the weighted averages

$$C_m=\frac{1}{\pi}\int_0^{2\pi}C_m(\theta)\sin^2\theta d\theta \tag{32}$$

and

$$C_d=+\frac{3}{4}\int_0^{2\pi}C_d(\theta)\,|\cos\theta|\cos^2\theta d\theta. \tag{33}$$

With the above possibilities in mind, it is preferable to adopt the expressions

$$\frac{F}{\rho U_m^2D}=A_1\sin\theta+B_1'\cos\theta\,|\cos\theta|+\Delta R \tag{34}$$

or

$$\frac{F}{\rho U_m^2D}=\frac{\pi}{4}C_m\frac{D\sigma}{U_m}\sin\theta-\frac{C_d}{2}|\cos\theta|\cos\theta+\Delta R, \tag{34a}$$

where A_1, B_1', C_m, and C_d are constant, and ΔR has the value

$$\Delta R=A_3\sin 3\theta+A_5\sin 5\theta+B_3'\cos 3\theta+B_5'\cos 5\theta. \tag{35}$$

The function ΔR will be referred to as the remainder function, and then this remainder function is obtained by subtracting the computed values of $A_1\sin\theta$ and $B_1'|\cos\theta|\cos\theta$ from the observed $F/\rho U_m^2D$. The remainder thus obtained may be examined in regard to its Fourier structure and also as to its magnitude.

4. Characteristics of the Experimental Waves

The region under the nodal area of a standing wave that may be realized in a rectangular vessel furnishes a velocity field of simple harmonic motion in the velocity component U. This circumstance is not seriously modified even when the surges are moderately high.

Taking the x-axis in the plane surface of the undisturbed water, the z-axis vertical and upwards and the origin at one end of the basin, (see fig. 2), the surface elevation as reckoned from the undisturbed level, according to the second-approximation theory, from Miche [16], is

$$h=a\cos kx\sin\sigma t+a\frac{ak}{4}N_1\cos 2kx-a\frac{ak}{4}N_2\cos 2kx\cos 2\sigma t, \tag{36}$$

where

$$N_1=\frac{\cosh 2kH}{\sinh 2kH}$$

and

$$N_2=\frac{\cosh^2 kH\,(\cosh 2kH+2)}{\sinh^2 kH\sinh kH}.$$

Here $k=\pi/L$, L being the length of the basin; $\sigma=2\pi/T$, T being the period of oscillation; H the depth of water; and a the semiwave height, that is, the mean value of the extreme end deflections in a cycle. The expression for the period is the same as in the first-approximation theory, that is,

$$\sigma^2=gk\tanh kH. \tag{37}$$

Focusing attention on the basin end $x=0$, the surface displacement is

$$h=a\sin\sigma t+a\frac{ak}{4}N_1-a\frac{ak}{4}N_2\cos 2\sigma t;\qquad x=0. \tag{38}$$

Thus, the maximum elevation, occurring at $t=\pi/2\sigma$, is

$$h_1=a+a\frac{ak}{4}[N_1+N_2], \tag{39}$$

and the maximum depression, at $t=3\pi/2\sigma$, is

$$h_2=-a+a\frac{ak}{4}[N_1+N_2].$$

The ratio of the elevation to the depression is

$$\frac{h_1}{h_2}=-\left(1+\frac{Hk}{4}[N_1+N_2]\frac{a}{h}\right)\Big/\left(1-\frac{Hk}{4}[N_1+N_2]\frac{a}{H}\right), \tag{40}$$

and accordingly its value increases with wave height.

The surface configuration for $t=0$ is

$$h=a\frac{ak}{4}[N_1-N_2\cos 2kx],\qquad t=0. \tag{41}$$

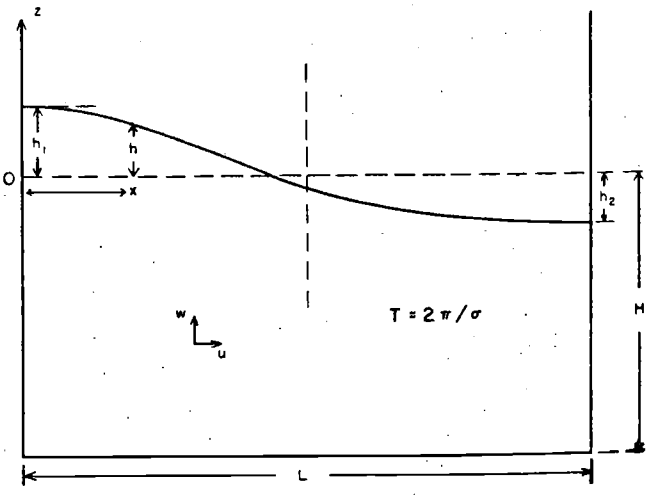

FIGURE 2. *Notation diagram for wave profile.*

This represents a positive hump at the center of the basin and depressions at the ends. As a result, the duration of time that the surface of the water at one end of the basin is found to be above the undisturbed level is shorter than the duration that it is below. This matter has a bearing on the manner of fixing the reference time of the force cycles studied, and requires further discussion.

At a small positive time $t=\tau_0$, the elevation h is nil, and this is the time when the wave in its upward surge reaches the undisturbed level.

Since $\sigma\tau_0$ is a small angle, $\sin \sigma\tau_0=\sigma\tau_0$, and from eq (38)

$$\sigma\tau_0=(N_2-N_1)\frac{ak}{4}-\frac{1}{2}(N_2-N_1)^2\frac{a^3k^3}{16}N_2. \tag{42}$$

At a later time, $t=T/2+\tau_1$, once more $h=0$. This is the time when the wave in its downward surge reaches the undisturbed level. Since $\sigma\tau_1$ is also a small angle, $\sin \sigma\tau_1=\sigma\tau_1$, and from eq (38)

$$\sigma\tau_1=(N_1-N_2)\frac{ak}{4}+\frac{1}{2}(N_1-N_2)^2\frac{a^3k^3}{16}N_2,$$

and, thus,

$$\tau_1=-\tau_0 \tag{43}$$

Let T_t denote the duration of time that the surface of the water at the end of the basin, $x=0$, is above the undisturbed level, and T_0 the duration below the same level. Accordingly,

$$T_t+T_0=T,$$

and

$$\frac{2(T_0-T_t)}{T}=2\left(1-\frac{2T_t}{T}\right).$$

By definition

$$T_t=\frac{T}{2}+\tau_1-\tau_0,$$

and in view of eq (43)

$$T_t=\frac{T}{2}-2\tau_0$$

or

$$\frac{2T_t}{T}=1-\frac{2\sigma\tau_0}{\pi}$$

and, thus

$$\frac{2(T_0-T_t)}{T}=\frac{4\sigma\tau_0}{\pi}.$$

Introducing the value of $\sigma\tau_0$ from eq (42)

$$\frac{2(T_0-T_t)}{T}=(N_2-N_1)\frac{kH}{\pi}\frac{a}{H}-(N_2-N_1)^2N_2\frac{H^3k^3}{8\pi}\left(\frac{a}{H}\right)^3. \tag{44}$$

If the instant when the upsurging wave at the end, $x=0$, reaches the level of the undisturbed water is observed, this then determines the instant $t=\tau_0$. Since $4\tau_0=T_0-T_t$, the value of τ_0 may be obtained from the time durations that the water surface is below or above the still level. If on the other hand these observations have not been made, then τ_0 must be obtained from eq (42), introducing in it the wave height a of the observed surge deflections.

The expressions for the particle velocities within the order of the approximations considered are from Miche [16],

$$u=\frac{gak}{\sigma}\frac{\cosh k(z+H)}{\cosh kH}\sin kx\cos\sigma t$$

$$-\frac{3}{4}\frac{ga^2k^2}{\sigma}\frac{\cosh 2k(z+H)}{\sinh^2 kH\sinh 2kH}\sin 2kx\sin 2\sigma t \tag{45}$$

and

$$w=\frac{gak}{\sigma}\frac{\sinh k(z+H)}{\cosh kH}\cos kx\cos\sigma t$$

$$+\frac{3}{4}\frac{g}{\sigma}a^2k^2\frac{\sinh 2k(z+H)}{\sinh^2 kH\sinh 2kH}\cos 2kx\sin 2\sigma t. \tag{46}$$

At the vertical plane through the midsection of the basin, that is, at the plane $x=L/2$ or $kx=\pi/2$, the velocities are

$$u=\frac{gak}{\sigma}\frac{\cosh k(z+H)}{\cosh kH}\cos\sigma t \tag{47}$$

and

$$w=-\frac{3}{4}\frac{g}{\sigma}a^2k^2\frac{\sinh 2k(z+H)}{\sinh^2 kH\sinh 2kH}\sin 2\sigma t. \tag{48}$$

Thus at the channel midsection, the horizontal component of the particle velocities is simple harmonic. The vertical component is also simple harmonic except that the frequency is twice as large. The effect of vertical velocity decreases with wave height. It is further reduced by lowering the object in the basin. Denoting the position of the object in the basin by z_1 and putting

$$U_m=\frac{gak}{\sigma}\frac{\cosh k(z_1+H)}{\cosh kH}, \tag{49}$$

the velocity components are

$$u=-U_m\cos\sigma t \tag{50}$$

and

$$w=-\frac{3}{4}kH\frac{\sinh k(z_1+H)}{\sinh^3 kH}\cdot\frac{a}{H}U_m\sin 2\sigma t. \tag{51}$$

It is inferred that w becomes less significant when kH is larger than 0.9. This limits the length of the basin for a given depth of water. For studies of wave forces in basins of greater length or with water of less depth the present theory proves inadequate.

All the experiments discussed subsequently were made in a basin of length $L=242$ cm and water

depth $H=70$ cm. The objects, cylinders or plates, were placed 25 cm below the water surface, that is $z_1=-25$ cm in the midsection plane $x_1=121$ cm.

For this condition, $Ik=0.908$, $N_1=1.054$, and $N_2=3.322$. From eq (40), the ratio of end deflections reduces to

$$\frac{h_1}{h_2}=-\frac{1+0.993\ a/H}{1-0.993\ a/H}. \tag{52}$$

The graph of this equation is shown in figure 3, and values from observation are given by circles. The agreement between theory and observation is satisfactory for a/H less than 0.3. With this restriction in mind, the value of the semiwave height a may be inferred from (39), that is,

$$\frac{h_1}{a}=1+0.993\ a/H. \tag{53}$$

During the tests the elevation h_1 was most easily observed.

From eq (49) the relation between the current semiamplitude and the wave height, in cgs units, is

$$U_m=3.43\ a. \tag{54}$$

At z_1 the horizontal velocity is not uniform in the vertical direction. In the absence of a cylinder, with z measured in centimeters,

$$\frac{1}{U_m}\frac{dU_m}{dz}=0.00685.$$

Thus, if ΔU_m be the difference in the maximum velocities at two points differing in elevation by D, then

$$\frac{\Delta U_m}{U_m}=0.48\ D/H.$$

For the largest cylinder used in the experiments, $D=7.62$ cm, the value of the ratio $\Delta U_m/U_m$ is 0.052.

The maximum value, during the cycle, of the vertical velocity component is given by

$$w_m/U_m=0.38\ a/H.$$

The majority of the experiments were made with a less than 10 cm. For these cases, w_m/U_m is less than 0.055.

From eq (44) the proportion of time that the surface of the water at one end of the channel is above or below the undisturbed level is given by

$$\frac{T_0-T_i}{T}=0.328\ \frac{a}{H}-0.254\left(\frac{a}{H}\right)^3. \tag{55}$$

The graph of this expression is shown in figure 4 and values from observation are given by circles. For the observations, there was introduced into the basin at each end a parallel-wire resistance electrode, the bare parts of the wires being about 5 cm long and placed in a horizontal position just touching the surface of water at rest. The time that the electric current was traversing the electrodes gave the time that the water surface was above the undisturbed level, as in figure 5.

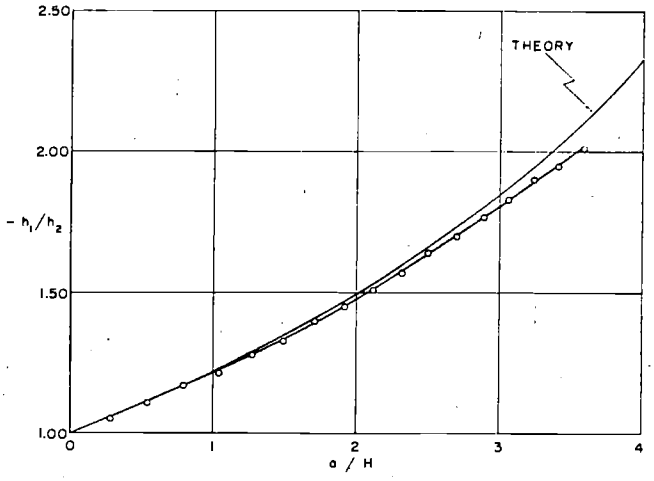

FIGURE 3. *Variation of end deflections with wave height.*

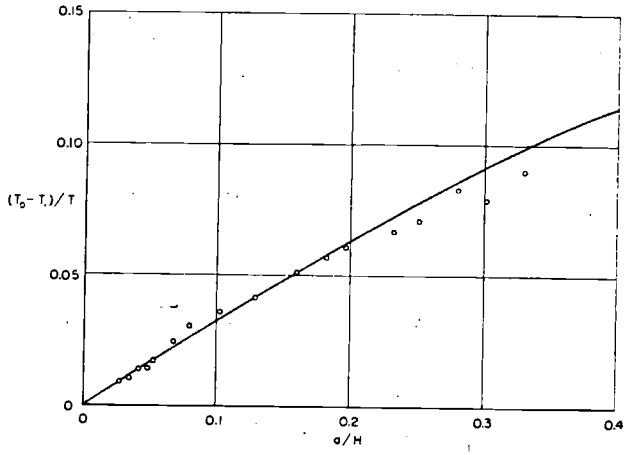

FIGURE 4. *Difference in the durations of the end elevations and depressions.*

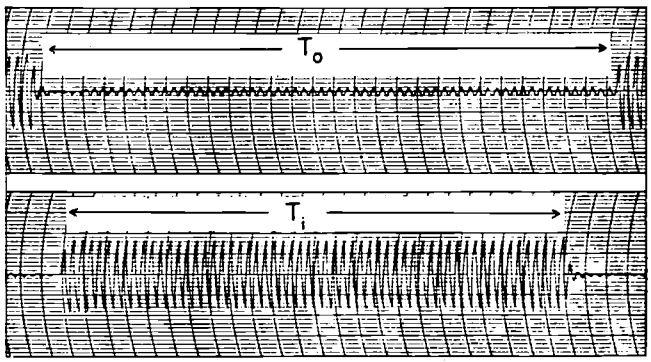

FIGURE 5. *Time record of the durations of the end deflections.*

5. Dynamometer and Calibration

The sketch of the dynamometer assembly is shown in figure 6. The rigid and massive base A for supporting purposes is firmly attached to the steel frame of the rocking basin directly above the water. The dynamometer itself consists of a pendular frame to which is attached the object to be immersed in water, a cylinder or a rectangular plate. The frame is constructed of brass angles and is strong enough to resist torsional and flexural deformation. The pivot depressions, located at the upper corners of the frame, consist of small bores of 1 mm in diameter in a bronze bedding. The bores are centered about polished steel conical points emerging from the supporting base. At a lower level two duraluminum annular rings of rectangular cross section are clamped to the frame and to the base.

These rings constitute elastic elements for measuring the forces. To indicate the ring deformations two pairs of strain gages, SR–4, 120 ohms, are glued to each of the rings, inside and outside, and at diametrically opposite points. The four strain gage elements form the bridge which is led to a universal analyser. The latter is relayed to one of the channels of a two-channel magnetic oscillograph. The second channel is reserved for timing observations. A similar connection is adopted for the other ring. By having four strain gages on each ring the sensitivity is increased and no corrections are needed for temperature changes. Two different sets of rings are used for measuring forces of different magnitudes. The method of calibration may be inferred from the sketch in figure 7. The sum of the forces on the two rings equals 0.625 times the load applied to the frame. The ring deformations are examined for loads producing tension and compression. The indications of the ring deformations as read from the oscillograph record are linear as shown in figure 7. The calibrations were repeated before each run to guard against accidental changes in the strain-gage behavior.

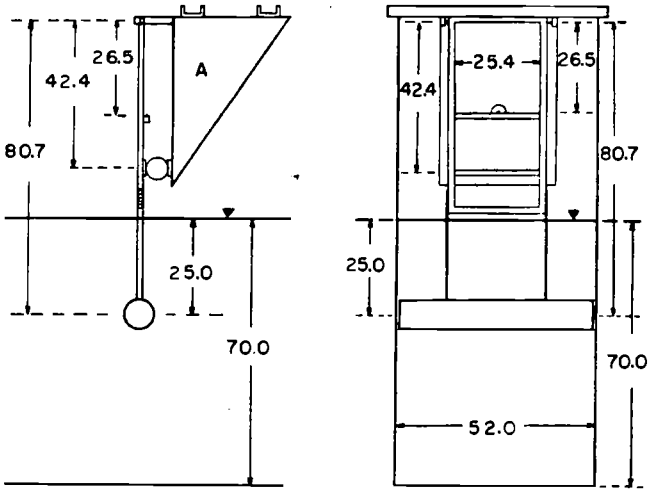

FIGURE 6. *Dynamometer assembly (dimensions in centimeters).*

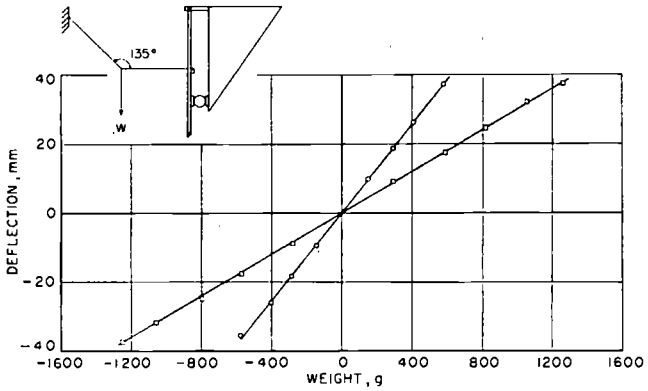

FIGURE 7. *Calibration of the strain gages.*

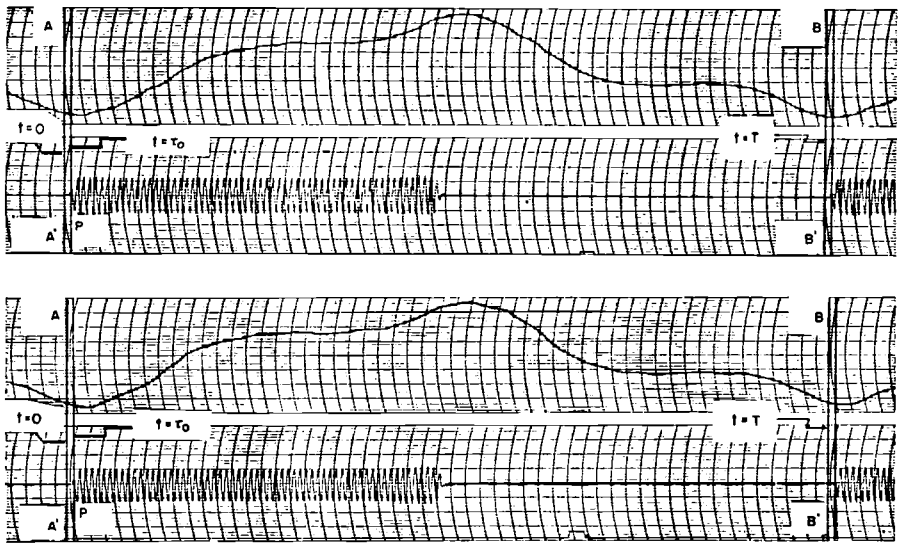

FIGURE 8. *An example of oscillograph record of forces.*

Run 82, $U_m T/D = 15.6$.

6. Record of Forces and the Reduction

An example of two oscillograph records of the forces, one from each ring, and of the timing is shown in figure 8. The nearly sinusoidal traces relate to the forces acting on the rings; the others, in steps, give the time sequence. The incidence of the larger deflections indicates the time that the parallel wire electrode at the basin end $x=0$ was immersed; and the incidence of no deflection indicates the time that the electrode was out of the water. The point P where the greater deflections appear to commence gives the instant that the upsurging water reached the undisturbed level. Thus the point P gives the time $t=\tau_0$, the value of which was computed from eq (55), $4\tau_0=T_0-T_t$, after introducing the semiwave height of the wave. This value was transferred to the record to mark the origin of time, $t=0$, shown by the line AA'. The line BB' indicates the end of the wave cycle and corresponds to $t=T$. To establish the correspondence of the records from the two rings, the timing marks appearing at the lower edges of the records were used.

At the time the record of the forces was being taken the wave elevation h_1 was read visually against a paper scale attached to the end wall of the basin. The water surface was readily discernable through the lucite walls of the basin. The magnitude of the semiwave height a was deduced from eq (53), using the observed value h_1. Maximum current U_m was deduced from eq (54).

The sum of the corresponding readings of the sinusoidal tracings in figure 8 gives the magnitude of the forces acting on the two rings when the calibration is applied. Taking moments about the dynamometer pivot point, the total force X on the cylinder is obtained. This is divided by the length of the cylinder to give F. The time history of the reduced force, $F/\rho U_m^2 D$, is shown in figure 9.

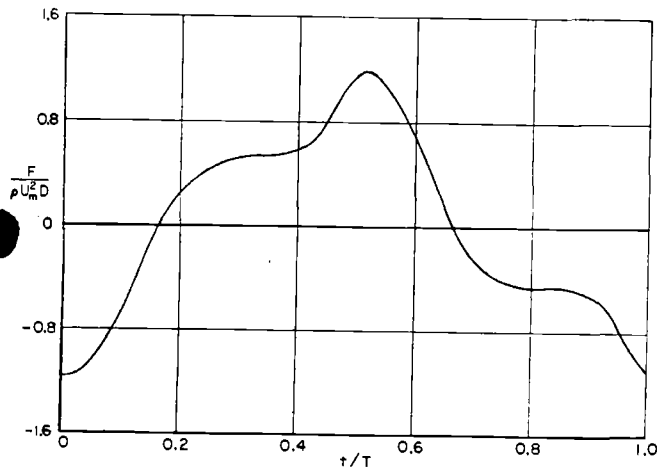

FIGURE 9. *An example of a curve of reduced forces on a cylinder.* Run 82. $U_mT/D=15.6$.

7. Inertia and the Drag Coefficients of Cylinders and Plates

Considering the force data in dimensionless form, such as shown in figure 9, the coefficients A_1 and B_1' of eq (34) were determined by the method implied in eq (30) and (31). The desired integrations were carried out in the form of summations by giving to the differential multiplier $d\theta$ the incremental value $\Delta\theta=0.05\pi$. The values of A_1 and B_1' thus found are entered in table 5 for the cylinders and in table 6 for the plates. Tables 1 and 2 contain the diameters of the cylinders, or the width of the plates, the values of the maximum currents and the water temperatures. Next the values of the inertia coefficient, C_m, were determined on the basis of eq (30), and the values of the drag coefficient, C_d, on the basis of eq (31). These results are entered in table 3 for the cylinders and in table 4 for the plates. These tables also contain the Reynolds number U_mD/ν and the period parameter U_mT/D.

The inertia coefficient C_m varies from the theoretical value 2 as the diameter of the cylinder is changed, or with a given cylinder as the maximum current is varied. Similar variations occur in the drag coefficient C_d, the changes being in the form of additions to the value experienced in steady flow. A correlation between the coefficients and Reynolds number U_mD/ν does not appear to exist. On the other hand, when these coefficients are related to the period parameter U_mT/D, definite and regular dependencies are found. This is illustrated in figures 10 and 11 for the cylinders, and in figures 12 and 13 for the plates.

TABLE 1. *Cylinders*

[T=2.075 sec]

Run	D	U_m	θ	Run	D	U_m	θ
	in.	*cm/sec*	° *C*		*in.*	*cm/sec*	° *C*
1	3	36.2	23.0	30	1	71.7	30.0
2	3	30.2	22.0	31	1	58.7	30.0
3	3	27.7	23.0	32	1	45.3	30.0
4	3	24.5	22.5	33	1	36.0	30.0
5	3	21.1	22.5	34	0.75	70.7	30.0
6	3	19.2	22.0	35	.75	63.8	30.0
7	3	15.8	22.0	36	.75	53.5	30.0
8	3	13.1	23.0	37	.75	45.3	30.0
9	3	10.0	23.0	38	.75	38.1	30.0
10	2.5	33.1	24.0	39	.5	73.4	30.0
11	2.5	27.4	24.0	40	.5	58.7	30.0
12	2.5	20.7	24.0	41	.5	48.0	30.0
13	2.5	13.0	24.0	78	1.75	27.6	22.6
14	2.5	10.3	24.0	79	1.75	24.0	22.0
15	2	41.5	24.0	80	1.75	17.7	22.0
16	2	35.4	24.0	81	1.75	14.4	22.0
17	2	27.5	24.0	82	1.5	28.7	20.5
18	2	19.1	24.8	83	1.5	25.2	20.5
19	2	23.5	24.8	84	1.5	20.2	20.5
20	1.5	53.2	26.0	85	1.5	14.6	20.5
21	1.5	43.4	26.0	86	0.5	66.4	21.0
22	1.5	33.4	26.0	87	.5	54.8	21.0
23	1.5	25.7	26.0	88	.5	44.6	21.0
24	1.5	19.4	26.0	89	.5	32.6	21.0
25	1.25	62.9	24.0	90	.75	54.0	12.0
26	1.25	54.5	28.0	91	.75	49.6	12.0
27	1.25	43.8	24.0	92	.75	46.0	12.0
28	1.25	35.7	29.2	93	.75	41.0	12.0
29	1.25	27.1	29.2				

TABLE 2. *Plates*

[T=2.075 sec]

Run	D	U_m	θ	Run	D	U_m	θ
	in.	*cm/sec*	° *C*		*in.*	*cm/sec*	° *C*
42	3	14.1	23.0	60	1.5	13.7	24.8
43	3	12.7	23.0	61	1.25	37.0	28.5
44	3	9.8	23.0	62	1.25	29.5	28.5
45	3	8.0	23.0	63	1.25	22.0	28.5
46	3	6.4	23.0	64	1.25	16.1	28.5
47	2.5	18.5	24.0	65	1	41.2	30.4
48	2.5	15.8	24.0	66	1	34.5	30.4
49	2.5	13.0	24.0	67	1	27.4	30.4
50	2.5	10.3	24.0	68	1	18.9	30.4
51	2.5	6.5	24.0	69	0.75	57.1	30.8
52	2	21.6	27.0	70	.75	47.0	30.8
53	2	18.9	27.0	71	.75	37.7	30.8
54	2	16.1	27.0	72	.75	27.4	30.8
55	2	13.0	27.0	73	.5	72.4	30.0
56	2	9.9	27.0	74	.5	63.6	30.0
57	1.5	30.0	24.8	75	.5	54.0	30.0
58	1.5	25.0	24.8	76	.5	45.3	30.0
59	1.5	18.9	24.8	77	.5	35.8	30.0

For the cylinders, as one passes from the small values of the period parameter to the larger values, the inertia coefficient commences to fall from the initial value 2 to a minimum value of 1.00 at $U_mT/D=15$ and then gradually increases to a value of 2.5 at $U_mT/D=120$. In regard to the coefficient of drag, there is an increase from the initial value 0.9 to a maximum value 2.5 at $U_mT/D=15$ and then there is a gradual decrease to the value obtained in steady flow. It appears that for the cylinders the narrow region around $U_mT/D=15$ is a critical one.

As regards the plates, the course of the variations of C_m and C_d with the period parameter is of a very different kind. It will be noticed that C_m first increases, then decreases and finally rises again to a value of nearly 4.5. The most remarkable behavior, however, is in regard to C_d. The coefficient of drag, starting with an unusually large value, 10, decreases rapidly at first and then gradually for

TABLE 3. *Cylinders*

Run	C_m	C_d	U_mT/D	U_mD/ν	Run	C_m	C_d	U_mT/D	U_mD/ν
1	1.11	1.24	9.9	293×10³	30	1.66	1.09	58.6	227×10³
2	1.44	1.14	8.2	239	31	1.70	1.29	47.9	185
3	1.49	1.32	7.6	225	32	1.68	1.40	37.0	143
4	1.70	1.13	6.7	196	33	1.64	1.49	29.4	114
5	1.88	1.00	5.7	169	43	1.82	1.10	77.0	167
6	1.95	0.91	5.2	152	35	1.61	1.19	69.5	151
7	2.05	1.23	4.3	125	36	1.63	1.42	58.3	127
8	2.10	1.01	3.6	106	37	1.64	1.45	49.3	107
9	2.14	0.70	2.7	81	38	1.84	1.50	41.5	90
10	0.74	1.69	10.8	229	39	2.54	1.07	119.9	116
11	1.14	1.61	8.9	189	40	2.35	1.29	95.8	93
12	1.71	1.36	6.8	143	41	2.15	1.42	78.5	76
13	2.02	1.15	4.3	90	78	0.82	1.99	12.9	127
14	2.06	1.12	3.4	71	79	.84	2.08	11.2	111
15	0.72	1.73	17.0	230	80	1.41	2.06	8.3	82
16	.70	1.98	14.5	196	81	1.78	1.75	6.7	67
17	.83	2.18	11.2	152	82	0.80	2.05	15.6	109
18	1.50	1.89	7.8	108	83	.78	2.28	13.7	96
19	1.10	1.97	9.6	132	84	.87	2.36	11.0	77
20	1.02	1.30	29.0	231	85	1.46	2.18	7.9	56
21	1.02	1.49	23.6	188	86	2.52	1.18	108.4	85
22	0.85	1.73	18.2	145	87	2.60	1.31	89.5	71
23	.74	2.15	14.0	112	88	2.32	1.43	72.9	57
24	.87	2.21	10.6	84	89	2.26	1.54	53.2	42
25	1.24	1.15	41.1	218	90	1.82	1.28	58.8	83
26	1.27	1.23	35.6	206	91	1.81	1.38	54.0	76
27	1.40	1.46	28.6	152	92	1.81	1.42	50.1	71
28	1.26	1.52	23.3	138	93	1.76	1.54	44.7	63
29	0.87	1.75	17.7	105					

TABLE 4. *Plates*

Run	C_m	C_d	U_mT/D	U_mD/ν	Run	C_m	C_d	U_mT/D	U_mD/ν
42	1.94	8.75	3.8	114×10²	60	2.51	5.15	7.5	58×10²
43	1.74	8.81	3.5	103	61	2.14	3.25	24.2	142
44	1.56	9.76	2.7	80	62	1.07	3.94	19.3	113
45	1.51	10.21	2.2	65	63	1.43	4.09	14.3	84
46	1.35	11.55	1.7	52	64	2.25	4.43	10.5	62
47	2.28	5.50	6.1	128	65	2.45	3.13	33.6	131
48	2.12	7.06	5.2	109	66	2.10	3.55	28.2	110
49	2.00	8.01	4.2	90	67	2.01	3.68	22.4	87
50	1.91	8.64	3.4	71	68	1.56	4.38	15.4	60
51	1.57	11.44	2.1	45	69	3.17	2.43	62.2	138
52	2.22	5.21	8.8	128	70	2.88	2.86	51.2	113
53	2.44	5.48	7.7	112	71	2.89	3.06	41.1	91
54	2.42	6.31	6.6	95	72	2.71	3.36	29.9	66
55	2.17	7.25	5.3	77	73	4.96	1.81	118.2	114
56	2.16	8.04	4.1	59	74	4.09	2.03	104.0	101
57	0.95	4.11	16.3	127	75	4.00	2.32	88.3	85
58	1.07	4.28	13.6	106	76	3.58	2.45	74.0	72
59	2.08	4.61	10.3	80	77	3.70	2.59	58.6	57

R_e

TABLE 5. *Cylinders*

Run	A_1	B_1'	A_3	B_3'	A_5	B_5'	U_mT/D
1	0.56	−0.62	−0.11	−0.04	−0.03	−0.08	9.0
2	.87	−.57	−.06	−.03	−.02	−.06	8.2
3	.97	−.66	−.08	.00	−.02	−.04	7.6
4	1.26	−.56	−.03	+.05	−.01	−.03	6.7
5	1.62	−.51	−.02	.05	.00	−.03	5.7
6	1.81	−.46	+.02	.06	.00	−.01	5.2
7	2.35	−.62	.01	.12	−.01	−.02	4.3
8	2.91	−.51	.03	.14	+.01	.00	3.6
9	3.87	−.35	.01	.08	−.02	+.02	2.7
10	0.34	−.84	−.19	−.02	−.04	−.08	10.8
11	.63	−.80	−.14	−.05	−.04	−.09	8.9
12	1.25	−.68	−.07	−.02	.00	−.06	6.8
13	2.34	−.58	+.10	+.13	+.01	−.01	4.3
14	3.03	−.56	.01	.14	.00	+.01	3.4
15	0.21	−.96	−.18	.00	−.04	−.05	17.0
16	.24	−.99	−.22	−.01	−.02	−.07	14.5
17	.36	−1.09	−.19	−.05	−.02	−.12	11.2
18	.95	−0.95	−.14	−.04	−.02	−.11	7.8
19	.57	−.99	−.15	−.06	−.01	−.11	9.6
20	.17	−.65	−.05	.00	−.01	−.03	29.0
21	.21	−.74	−.07	.00	.00	−.04	23.6
22	.23	−.87	−.15	−.05	−.04	−.07	18.2
23	.26	−1.08	−.22	−.04	.00	−.08	14.0
24	.41	−1.10	−.20	−.07	.00	−.11	10.6
25	.15	−0.58	.00	+.01	.00	−.01	41.1
26	.18	−.62	−.01	.01	.00	−.02	35.6
27	.24	−.73	−.01	.02	.00	−.02	28.6
28	.27	−.76	−.04	.00	.00	−.05	23.3
29	.24	−.87	−.13	−.04	−.04	−.07	17.7
30	.14	−.55	+.02	+.01	.00	−.01	58.6
31	.17	−.64	.02	.01	−.01	−.01	47.9
32	.22	−.70	.01	.03	.00	−.02	37.0
33	.27	−.74	.01	.02	.00	−.02	29.4
34	.12	−.55	.03	.01	−.01	−.01	77.0
35	.11	−.60	.01	.01	−.01	−.01	69.5
36	.14	−.71	.01	.02	.00	−.02	58.3
37	.16	−.72	.01	.02	−.01	−.01	49.3
38	.22	−.75	.02	.02	.00	−.01	41.5
39	.10	−.54	.03	.00	.00	−.01	119.9
40	.12	−.65	.02	.01	.00	−.01	95.8
41	.14	−.71	.01	.02	.00	−.01	78.5
78	.31	−.99	−.18	−.05	−.01	−.10	12.9
79	.37	−1.04	−.19	−.02	−.03	−.12	11.2
80	.84	−1.03	−.15	−.10	−.01	−.13	8.3
81	1.30	−0.88	−.07	−.10	.00	−.10	6.7
82	0.25	−1.02	−.22	−.03	−.04	−.06	15.6
83	.28	−1.14	−.24	−.01	−.01	−.10	13.7
84	.39	−1.18	−.23	−.05	−.02	−.14	11.0
85	.91	−1.09	−.15	−.04	.00	−.12	7.9
86	.11	−0.59	+.03	+.01	.00	−.01	108.4
87	.14	−.65	.02	.01	−.01	−.01	89.5
88	.16	−.72	.01	.02	−.01	−.01	72.9
89	.21	−.77	.01	.04	+.01	−.01	53.2
90	.15	−.64	.02	.01	.00	−.01	58.5
91	.17	−.69	.02	.01	.00	−.01	54.0
92	.18	−.71	.02	.02	.00	.00	50.1
93	.19	−.77	.02	.02	.00	−.01	44.7

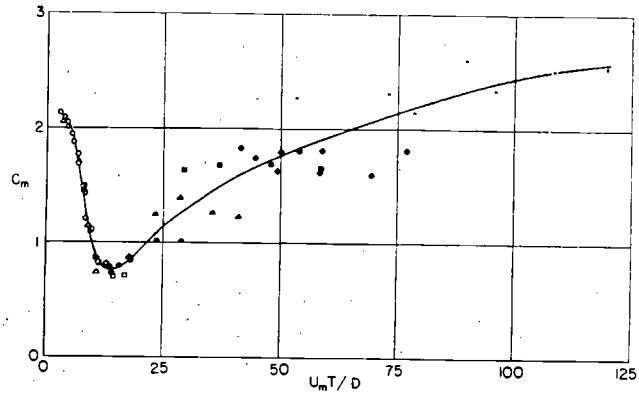

FIGURE 10. *Variation of inertia coefficient of cylinders.*
Diameter (inches): 3 2.5 2 1.75 1.5 1.25 1 0.75 0.5
Corresponding symbol: ○ △ □ ◇ ● ▲ ■ ◆ +

TABLE 6. *Plates*

Run	A_1	B_1'	A_3	B_3'	A_5	B_5'	U_mT/D
42	2.50	−4.38	0.58	0.56	0.01	−0.05	3.8
43	2.49	−4.41	.58	.47	.04	−.11	3.5
44	2.86	−4.88	.47	.40	−.02	−.18	2.7
45	3.42	−5.11	.53	.45	−.01	−.17	2.2
46	3.83	−5.77	.43	.48	−.02	−.16	1.7
47	1.86	−2.75	.37	.58	−.08	−.03	6.1
48	2.03	−3.53	.45	.59	−.04	−.02	5.2
49	2.32	−4.01	.53	.64	−.02	−.02	4.2
50	2.81	−4.32	.68	.52	+.07	−.06	3.4
51	3.63	−5.72	.61	.55	.01	−.14	2.1
52	1.24	−2.61	.35	.42	−.05	+.02	8.8
53	1.56	−2.74	.31	.49	−.06	−.03	7.7
54	1.81	−3.16	.38	.56	−.05	−.02	6.6
55	2.01	−3.63	.45	.54	−.01	−.03	5.3
56	2.63	−4.02	.66	.60	.00	−.01	4.1
57	0.29	−2.05	.29	.33	+.02	+.07	16.3
58	.39	−2.14	.30	.31	.00	.03	13.6
59	1.00	−2.31	.29	.43	−.08	.00	10.3
60	1.66	−2.58	.30	.54	−.07	−.04	7.5
61	0.44	−1.62	.11	.18	−.05	−.02	24.2
62	.27	−1.97	.18	.19	+.02	+.07	19.3
63	.49	−2.04	.31	.36	−.02	.04	14.3
64	1.05	−2.22	.30	.45	−.06	−.01	10.5
65	0.36	−1.56	.08	.13	−.05	−.01	33.6
66	.37	−1.77	.09	.16	−.04	−.01	28.2
67	.44	−1.84	.16	.19	−.02	+.03	22.4
68	.50	−2.19	.32	.38	−.01	.06	15.4
69	.25	−1.21	.05	.05	−.02	−.04	62.2
70	.28	−1.43	.06	.08	−.03	−.04	51.2
71	.35	−1.53	.08	.11	−.04	−.04	41.1
72	.45	−1.68	.11	.13	−.03	−.01	29.9
73	.21	−0.91	.06	.03	−.01	−.03	118.2
74	.19	−1.01	.06	.03	−.01	−.03	104.0
75	.22	−1.16	.05	.05	−.02	−.03	88.3
76	.24	−1.22	.05	.05	−.02	−.02	74.0
77	.31	−1.29	.07	.06	−.03	−.03	58.6

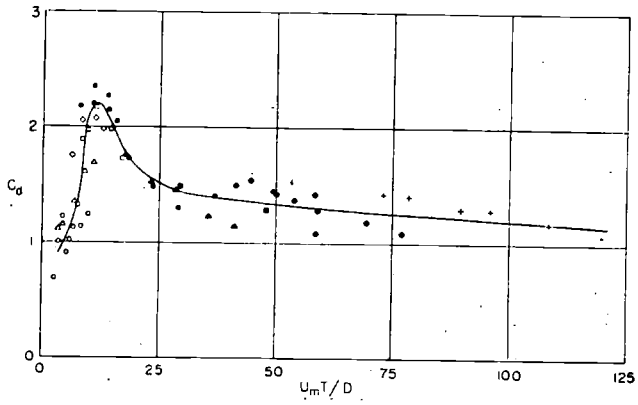

FIGURE 11. *Variation of drag coefficient of cylinders.*
Diameter (inches): 3 2.5 2 1.75 1.5 1.25 1 0.75 0.5
Corresponding symbol: ○ △ □ ◇ ● ▲ ■ ◆ +

increasing period parameter. The final value is almost identical with that found for steady flow. It is perhaps important to mention that O'Brien and Morison [17] noted equally large values of drag coefficients for spheres subjected to the action of progressive waves. It will be noted that the larger values of C_d are associated with the smaller values of C_m, and the larger values of C_m with the smaller values of C_d. Because the drag coefficient is large when U_mT/D is small and the variation of C_m is relatively moderate, the wave forces on plates are essentially due to drag, and the inertia effects play a small role almost independent of the period parameter.

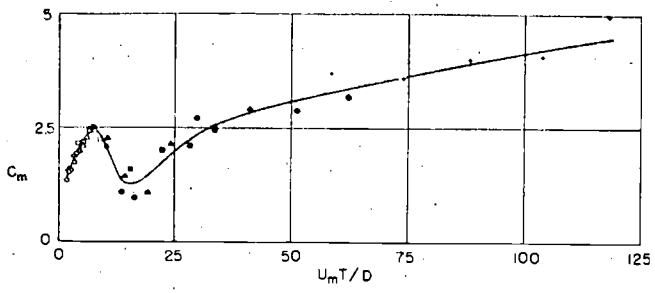

FIGURE 12. *Variation of inertia coefficient of plates.*

Diameter (inches): 3 2.5 2 1.5 1.25 1 0.75 0.5
Corresponding symbol: ○ △ □ ● ▲ ■ ◆ +

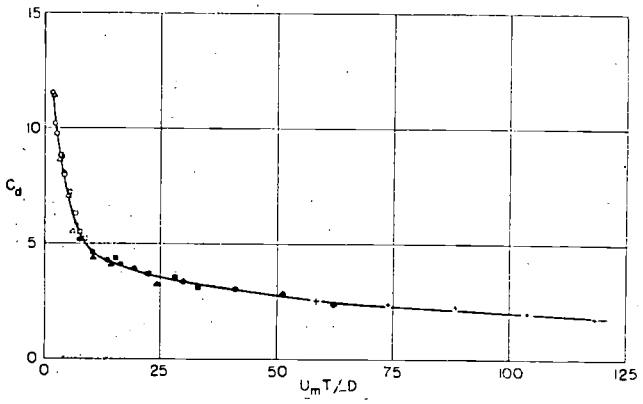

FIGURE 13. *Variation of drag coefficient of plates.*

Diameter (inches): 3 2.5 2 1.5 1.25 1 0.75 0.5
Corresponding symbol: ○ △ □ ● ▲ ■ ◆ +

8. Variations of the Remainder Function and C_m and C_d During the Wave Cycle

The values of C_m and C_d given in tables 3 and 4 are average values for the entire wave cycle, and in some cases local values may differ from the average. Where the inertia and drag coefficients, C_m and C_d, each have the same constant value at all phases of the wave cycle, eq (24) should suffice to describe adequately the magnitude of the forces at every phase. On the other hand, should C_m and C_d vary with the different phases, the forces are better represented by eq (34a). The variations in C_m and C_d should lead to the remainder force function ΔR. The examples of the remainder function ΔR are given in figures 14 and 15 where ΔR is the difference between $F/\rho U_m^2 D - A_1 \sin\theta$ and $B_1' \cos\theta \mid \cos\theta \mid$ in conformity with eq (34). Once a curve of ΔR as a function of θ is obtained, its structure in Fourier components may be considered and the coefficients A_3, A_5 . . ., and B_3', B_5' may be obtained. These determinations are given in tables 5 and 6 and in figures 16, 17, 18, and 19.

Now for the determinations of the local values of C_m and C_d, two methods are available. The first gives the point values of the coefficients in a wave cycle as determined from the observed values of $F/\rho U_m^2 D$, using eq (24). Two sets of evaluations

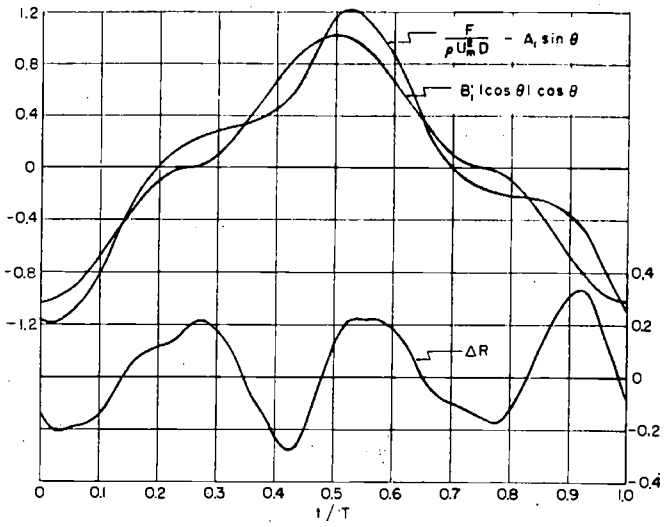

FIGURE 14. *Evaluation of remainder force ΔR for a cylinder.*
Run 82, $U_mT/D = 15.6$.

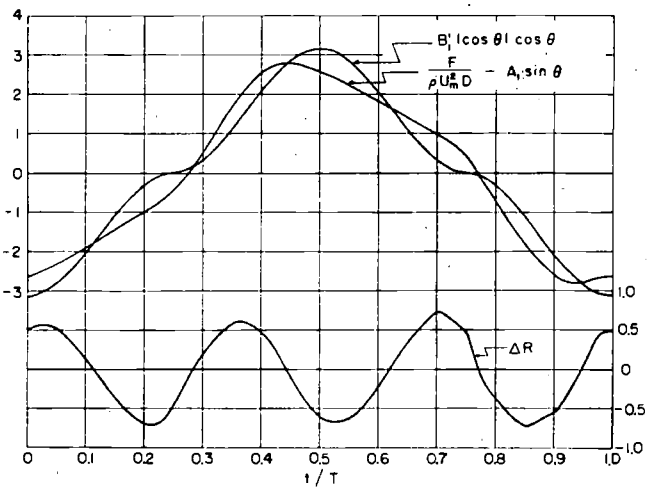

FIGURE 15. *Evaluation of remainder force ΔR for a plate.*
Run 54, $U_mT/D = 6.6$.

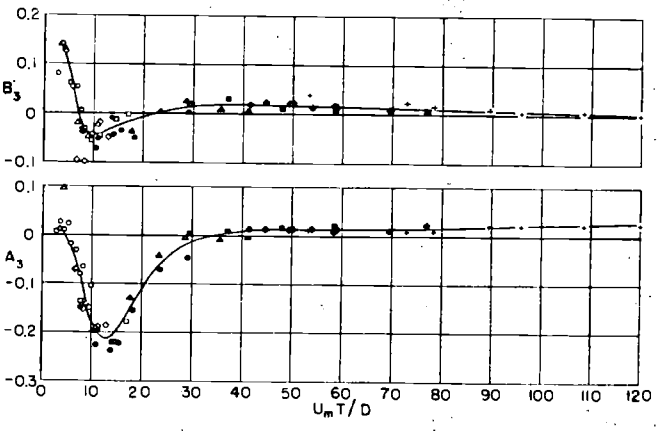

FIGURE 16. *Variation of coefficients of the remainder force of cylinders.*

Diameter (inches): 3 2.5 2 1.75 1.5 1.25 1 0.75 0.5
Corresponding symbol: ○ △ □ ◇ ● ▲ ■ ◆ +

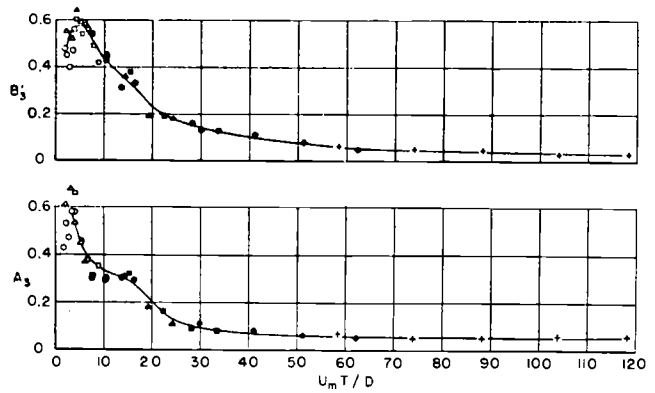

FIGURE 17. *Variation of coefficients of the remainder force of plates.*

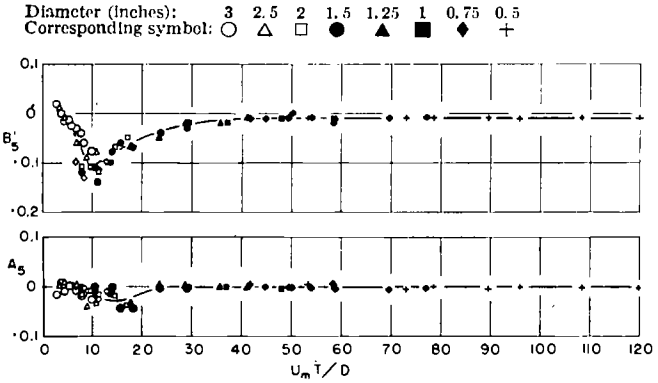

FIGURE 18. *Variation of coefficients of the remainder force of cylinders.*

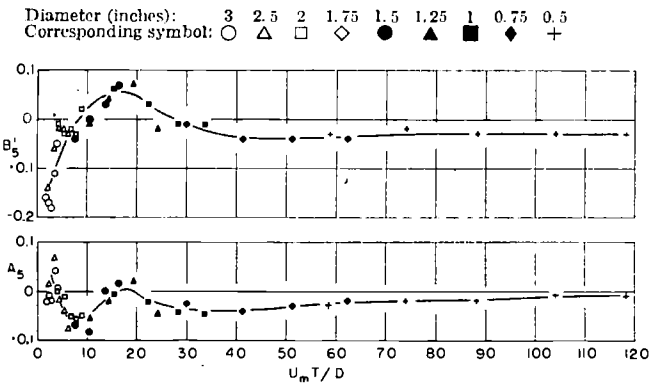

FIGURE 19. *Variation of coefficients of the remainder force of plates.*

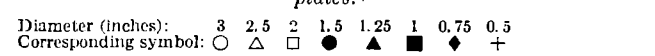

were made, the basic suppositions being as follows: It was assumed in the first evaluation that for $\theta_1=\pi/2+\alpha$ and $\theta_2=\pi/2-\alpha$, where α is an angle less than $\pi/2$, the coefficients C_m and C_d each have equal values, since these are the phases where the accelerations, du/dt, are equal, and the currents u, are equal in absolute value although of opposing signs. This is true also for $\theta_1=3\pi/2+\alpha$ and $\theta_2=3\pi/2-\alpha$. In the second evaluation, it was assumed that for $\theta=\pi+\beta$ and $\theta=\pi-\beta$, where β is an angle less than π, the coefficients C_m and C_d each have equal values, since these are the phases where the currents, u, are equal and the accelerations, du/dt, are equal in absolute value, although of opposing signs. Also since we know the values of the coefficients A_1, A_3, A_5 and B_1', B_3', B_5', the curves of C_m and C_d as function of θ may be obtained by using eq (28) and (29). The latter is the second method and is mathematically equivalent to the assumptions made above.

In the cylinder data the agreement between the observed and computed force is satisfactory when U_mT/D is small. The computation was based on eq (24), introducing the values of C_m and C_d from the tables. Figure 20 illustrates this agreement. The local values of $C_m(\theta)$ and $C_d(\theta)$ for this case are shown in figure 21. The first determinations discussed above are shown by circles and squares, whereas the curves are determined by the second method. It is seen that $C_m(\theta)$ is independent of the phase t/T and that the coefficient $C_d(\theta)$ is constant except in short ranges of the phases $t/T=0.25$ and 0.75. This is expected, for at these phases the current u vanishes. The values of C_m and C_d determined by eq (30) and (31) are given in the caption.

The agreement between the observed and computed forces is also satisfactory when the period parameter is large. This is illustrated in figure 22. The local values of the coefficients for this case are shown in figure 23. Here again, allowing small deviations, $C_m(\theta)$ is practically independent of the phase t/T and differs very little from the value given in table 3. On the other hand, considerable variations are obtained between the observed and computed values of the forces in those cases where the period parameter is near $U_mT/D=15$, as shown in figure 24. The local values of the coefficients for this case are shown in figure 25. Now $C_m(\theta)$ varies considerably with the phase t/T, the smaller values occurring at $t/T=0.0$, 0.50, and 1, and the larger values at $t/T=0.25$ and 0.75. Also, $C_d(\theta)$ appears to be considerably augmented at the phases where the velocity u vanishes, that is, at $t/T=0.25$ and 0.75. The example shown is typical for all the cases where U_mT/D is in the neighborhood of $U_mT/D=15$. In the example shown in figure 25, $C_m(\theta)$ shows large negative values at the points $t/T=0$, 0.5, and 1.0. The significance of this is not clear. It is believed, however, that the presence of negative values is not related altogether to the observational methods that were used.

For the plates deviations were always found between the observed values of the forces and the values computed on the basis of eq (24). An example is given in figure 26. The local values of $C_m(\theta)$ and $C_d(\theta)$ for this case are shown in figure 27. An additional example is given in figure 28. What is shown in these figures is typical for all the runs made with the plates. The coefficient $C_m(\theta)$ undergoes considerable variation in value for varying t/T, the greater values occurring at $t/T=0$, 0.5, and 1.0 and the lesser values at $t/T=0.25$ and 0.75. Furthermore, the increase in $C_d(\theta)$ at the points $t/T=0.25$ and 0.75 is very decided.

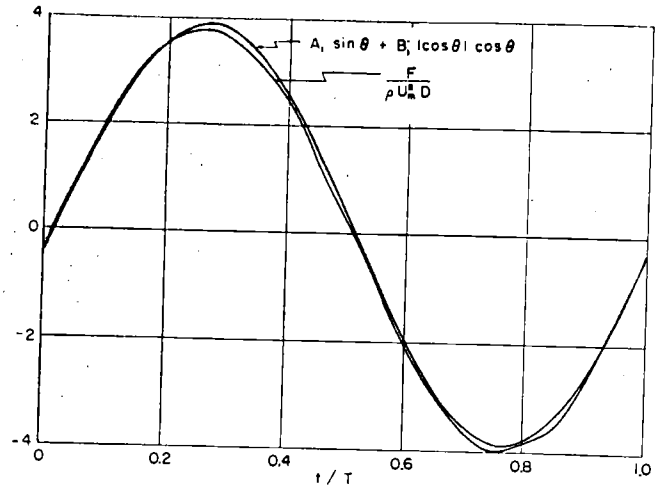

FIGURE 20. *Comparison of measured and computed forces on a cylinder.*
Run 9, $U_mT/D=3.0$.

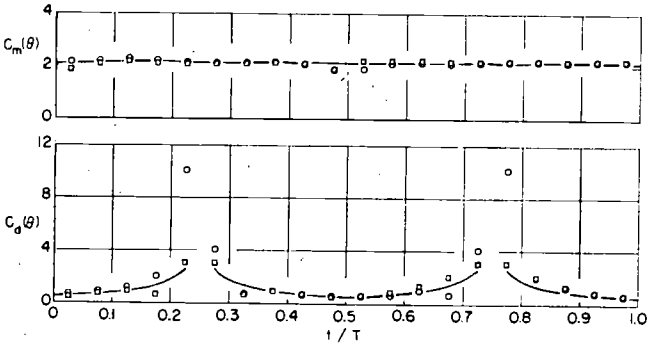

FIGURE 21. *An example of variation of the inertia and drag coefficients of a cylinder during a wave cycle.*
Run 9, $U_mT/D=3.0$, $C_m=2.14$, $C_d=0.70$.

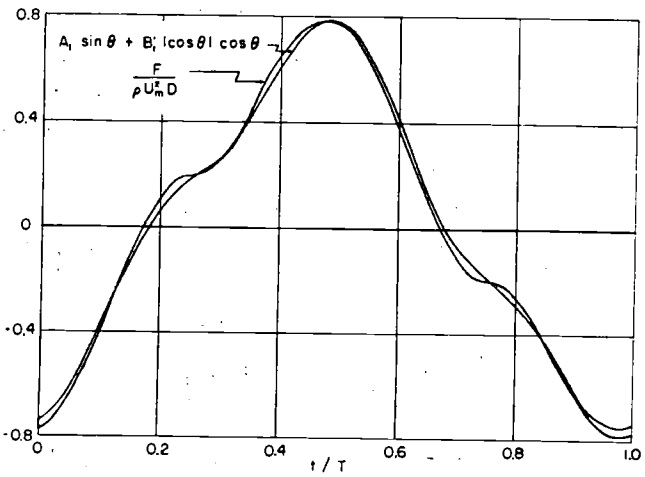

FIGURE 22. *Comparison of measured and computed forces on a cylinder.*
Run 93, $U_mT/D=44.7$.

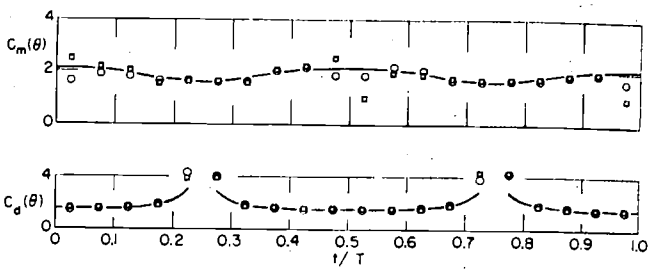

FIGURE 23. *An example of variation of the inertia and drag coefficients of a cylinder during a wave cycle.*
Run 93, $U_mT/D=44.7$, $C_m=1.76$, $C_d=1.54$.

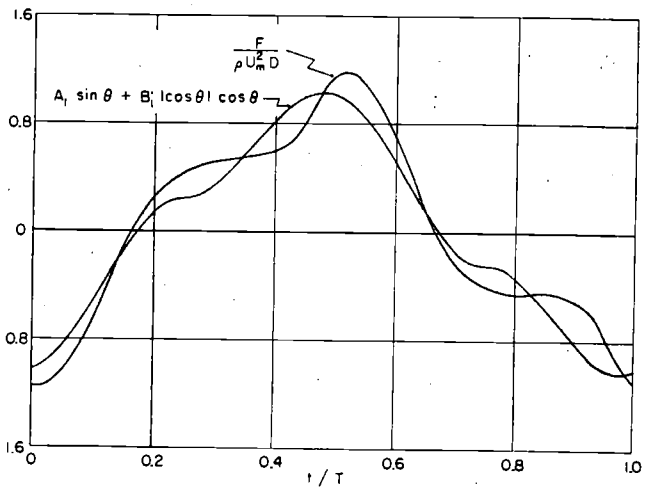

FIGURE 24. *Comparison of measured and computed forces on a cylinder.*
Run 82, $U_mT/D=15.6$.

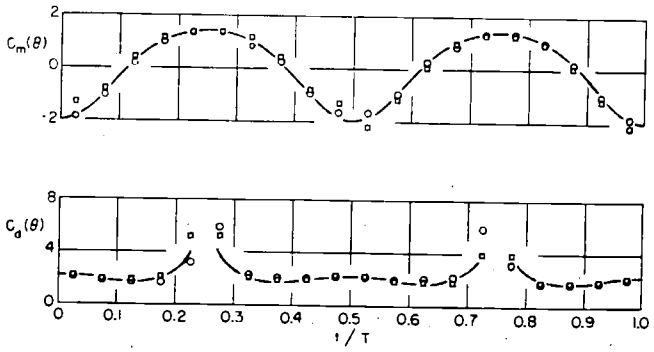

FIGURE 25. *An example of variation of the inertia and drag coefficients of a cylinder during a wave cycle.*
Run 82, $U_mT/D=15.6$, $C_m=0.80$, $C_d=2.05$.

For the cylinder data, as long as the period parameter is sufficiently small, or sufficiently large, the forces may be computed on the basis of eq (24); the remainder function, ΔR, is small. For period parameters in the neighborhood of the critical value, $U_mT/D=15$, the representation of forces is more exact using eq (34a); the remainder function is of significance. For the plate data the remainder may not be disregarded, in particular when the period parameter is small.

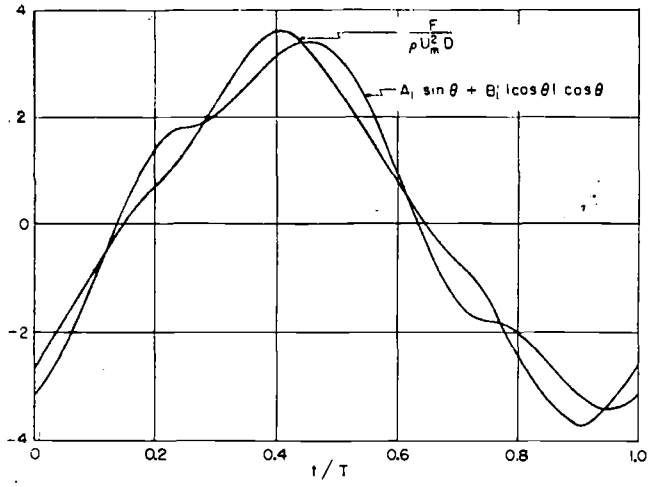

FIGURE 26. *Comparison of measured and computed forces on a plate.*

Run 54, $U_mT/D=6.6$.

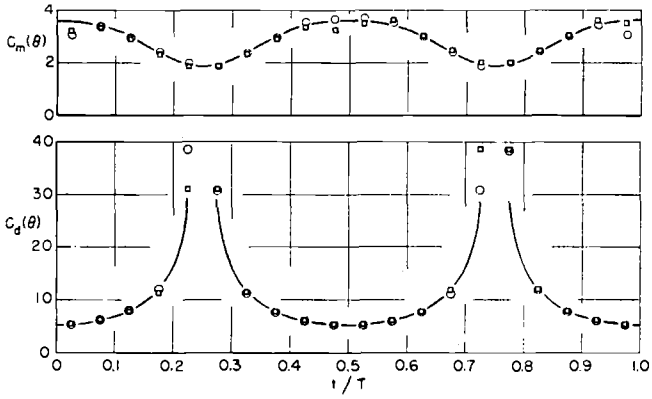

FIGURE 27. *An example of variation of the inertia and drag coefficients of a plate during a wave cycle.*

Run 54, $U_mT/D=6.6$, $C_m=2.42$, $C_d=6.31$.

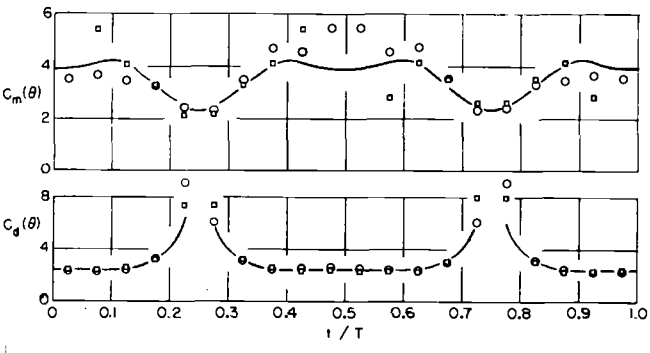

FIGURE 28. *An example of variation of the inertia and drag coefficients of a plate during a wave cycle.*

Run 69, $U_mT/D=62.2$, $C_m=3.17$, $Cd=2.43$.

9. Flow Pattern Around Cylinders and Plates

The flow patterns around the cylinders and plates for varying values of U_mT/D were examined, because they may have had a bearing on the fact that the nature of forces during a cycle is significantly affected by the period parameter. The flow pattern was visually examined by introducing a jet of colored liquid on one side of the immersed object. The disposition of the liquid close to the object during the cyclic motion was recorded by a still camera and also by a motion-picture camera. Some of these pictures are shown in figures 29 and 30.

Figure 29, a and b, were taken with the 3-inch cylinder, the first corresponding to $U_mT/D=4$, the second to a larger value $U_mT/D=10$. When the period parameter is small there is no separation of flow; the liquid near the cylinder clings to the cylinder, and the partitioning of flow from above and below is symmetrical. It will be remembered that at low period parameter the inertia coefficient is about equal to the theoretical value 2, and drag is negligible. As U_mT/D is increased there is separation of flow at the top surface of the cylinder during the relatively longer time that the flow continues in one direction. Although not visible in the picture, somewhat later, but prior to the reversal of current, liquid coming around the cylinder from below moves upward and, although transforming into an eddy, remains close to the cylinder.

Figure 29, c, illustrates the flow pattern for $U_mT/D=17$ with the 2-inch cylinder. Note the complete separation at the upper surface of the cylinder with the following flow around the lower surface directed upward with the subsequent eddy formation.

A completely different picture is obtained for large period parameter, as shown in figure 29, d, taken with the ½-inch cylinder, $U_mT/D=110$. Here one is confronted with the regular Karman vortices. The eddies are separated alternately from above and below.

With plates the flow patterns are decidedly different, especially for small period parameter. Figure 30, a and b, show the 3-inch plate, the first corresponding to $U_mT/D=1$, the second to a larger value, $U_mT/D=4$. Eddies are formed almost simultaneously at the upper and lower edges of the plates. For the smaller value of U_mT/D the eddies are apparently concentrated nearer the edges of the plate. Perhaps the large values of the drag coefficient for small period parameter are associated with the behavior of the eddies in this case, but the question is left open for another occasion.

Figure 30, c, illustrates the flow pattern for $U_mT/D=15$ with the 1½-inch plate. Here the eddy formation is no longer symmetrical, the separation occurring first at the upper edge of the plate followed by an eddy formed at the lower edge, remaining close to the plate.

Again the Karman vortices are obtained for large period parameter as shown in figure 30d taken with the ½-inch plate, $U_mT/D=110$.

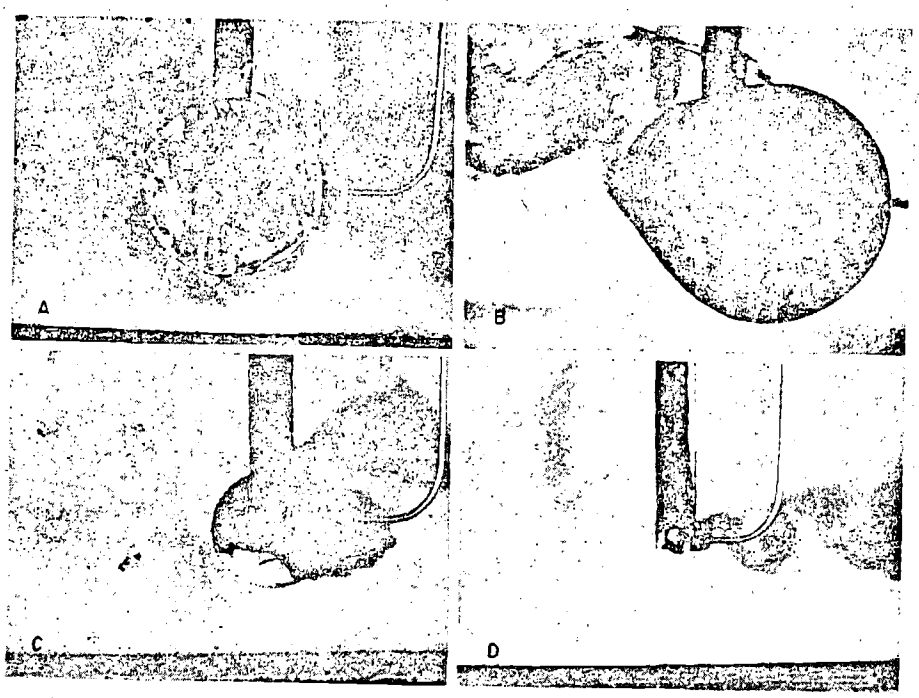

FIGURE 29. *Flow patterns around cylinders.*

(A) D=3 in., $U_m T/D$=4; (B) D=3 in., $U_m T/D$=10;
(C) D=2 in., $U_m T/D$=17; (D) D=0.5 in., $U_m T/D$=110.

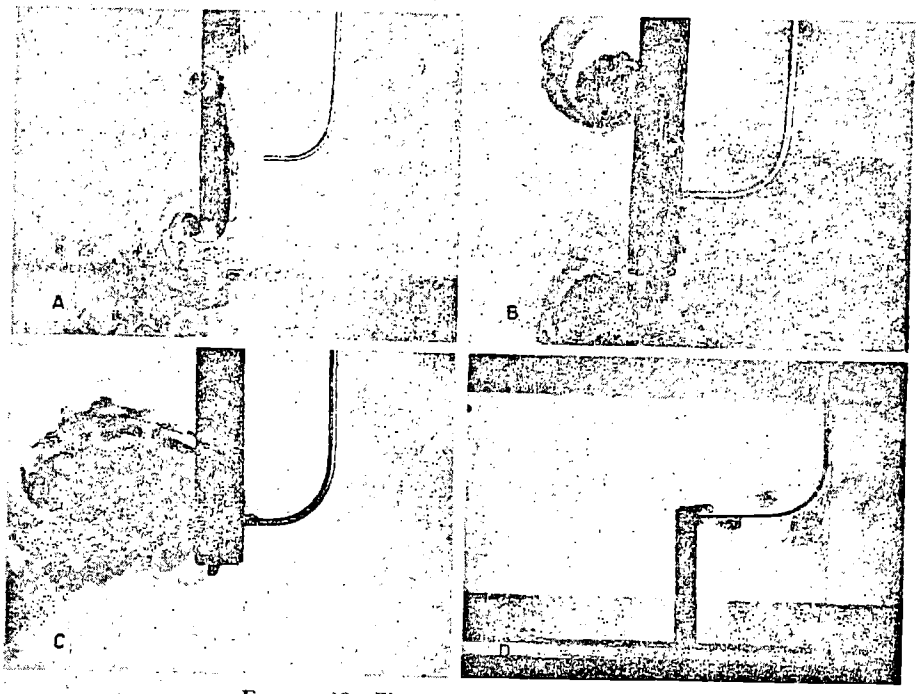

FIGURE 30. *Flow patterns around plates.*

(A) D=3 in., $U_m T/D$=1; (B) D=3 in., $U_m T/D$=4;
(C) D=1.5 in., $U_m T/D$=15; (D) D=0.5 in., $U_m T/D$=110.

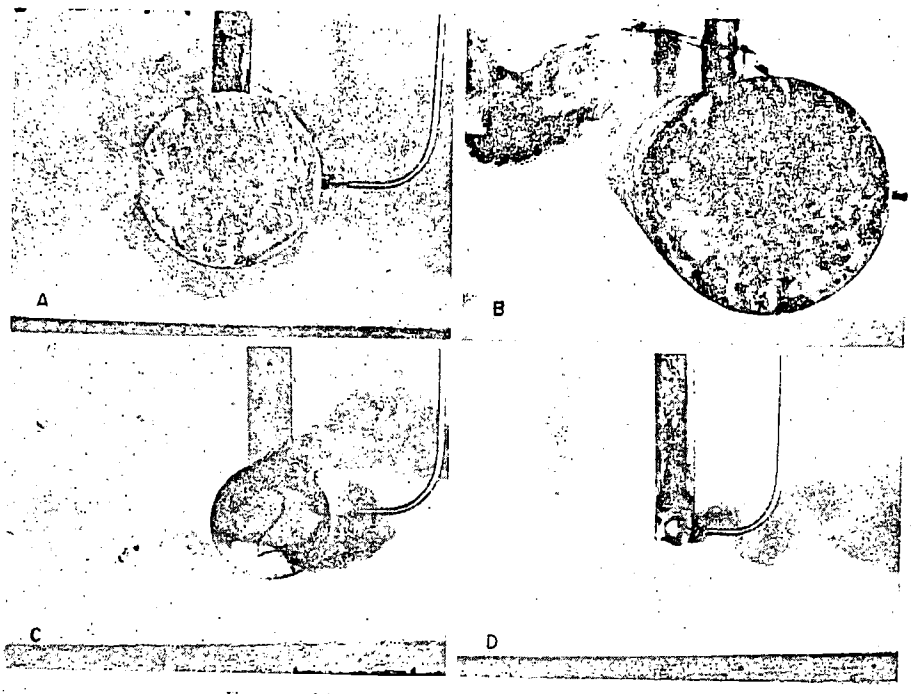

FIGURE 29. *Flow patterns around cylinders.*
(A) D=3 in., $U_m T/D$=4; (B) D=3 in., $U_m T/D$=10;
(C) D=2 in., $U_m T/D$=17; (D) D=0.5 in., $U_m T/D$=110.

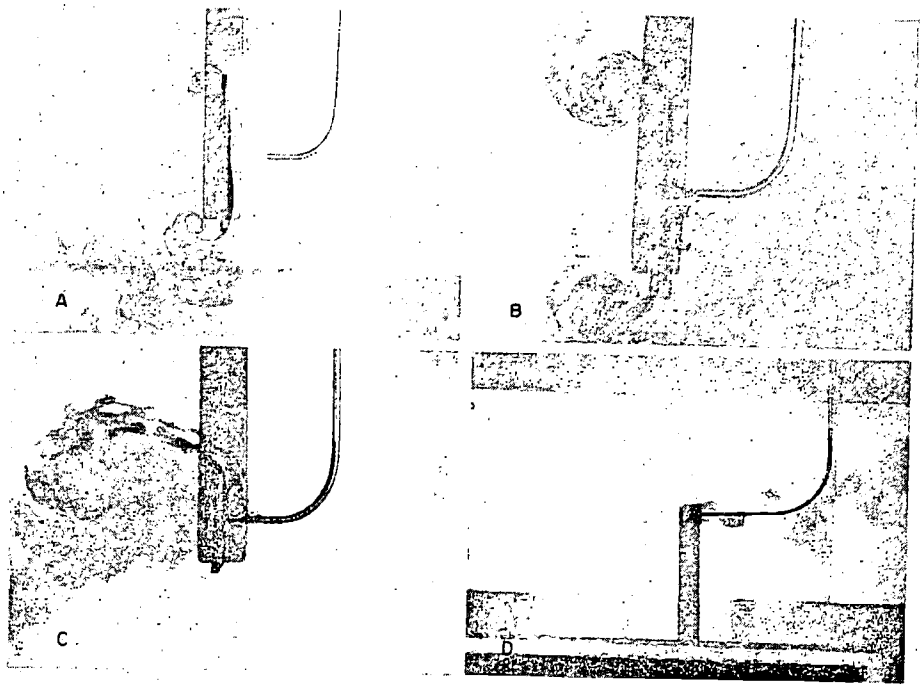

FIGURE 30. *Flow patterns around plates.*
(A) D=3 in., $U_m T/D$=1; (B) D=3 in., $U_m T/D$=4;
(C) D=1.5 in., $U_m T/D$=15; (D) D=0.5 in., $U_m T/D$=110.

The eddy appearances discussed above suggest the following interpretation as to the physical meaning of U_mT/D. If one defines a length, l, as the distance that a fluid particle would move in one direction in the absence of the cylinder, $l=U_mT/\pi$. Thus,

$$\frac{U_mT}{D}=\frac{\pi l}{D},$$

and accordingly the period parameter is proportional to the ratio of the distance traversed by a particle during a half cycle to the diameter of the cylinder. When the period parameter equals 15, l/D is 4.8. Perhaps when U_mT/D is smaller than 15, the distance traveled by a particle is not large enough to form complete eddies. When it equals 15, the distance suffices to form a single eddy, and when much larger than 15 the greater distances allow the formation of numerous vortices of the Karman vortex street. One can hardly refrain from pointing to the similarity between the period parameter and the Strouhal number, and as suggested by McNown and Keulegan [18], the product of Strouhal and period parameter numbers furnishes an alternate parameter as serviceable as the period parameter number. If T_s be the duration for the shedding of a single eddy, then the Strouhal number $fD/U=S$ may be written as $D/(2T_sU)=S$, since the number of alternative eddies shed during a second is $2f$ and $2fT_s$ equals 1 second. One may suppose that the relation is satisfied approximately also for sinusoidal motions, provided U is replaced by $U_m/2$. Hence, the Strouhal number for sinusoidal motion is $D/(U_mT_s)=S$.

Multiply the two sides by the wave parameter number U_mT/D,

$$\frac{T}{T_s}=S\frac{U_mT}{D}.$$

For cylinders, ignoring the dependence of S on the Reynolds number,

$$T/T_s=0.2\frac{U_mT}{D}.$$

As noted previously for the cylinders, C_m attains its least value, slightly less than unity, at about $U_mT/D=12.5$. This corresponds to the condition that $T/T_s=2$, nearly, and suggests that during a half cycle, that is, during a complete motion of fluid particle in one direction, a single eddy is formed and is separated (see also the figure 29, b). Obviously, the process of eddy shedding has a very significant bearing on the variations of the so-called coefficients of mass and drag, and account needs to be taken of this in the theoretical formulation of the basic process.

10. Maximum Force During a Wave Cycle

In engineering applications the main interest is in the magnitude of the maximum force experienced during a wave cycle. If the remainder function is neglected, the expression

$$F/\rho U_m^2D=A_1\sin\theta+B_1'|\cos\theta|\cos\theta$$

instead of the eq (24), may be utilized to evaluate the maximum force F_m and also its phase. If the maximum force $F_m/\rho U_m^2D$ occurs at $\theta=\theta_m$, the phase may be defined as

$$\Phi=\pi-\theta_m.$$

The maximum value of the computed force is given by

$$\frac{F_m}{\rho U_m^2D}=A_1\sin\theta_m+B_1'|\cos\theta_m|\cos\theta_m,$$

where θ_m satisfies the relation

$$A_1+2B_1'\sin\theta_m=0,\text{ or }\sin\theta_m=-\frac{A_1}{2B_1''},\qquad\text{for }\frac{\pi}{2}<\theta_m<\frac{3\pi}{2}.$$

As the coefficients A_1 and B_1'' are functions of U_mT/D only, then $F_m/\rho U_m^2D$ and Φ both are functions of U_mT/D. For greater accuracy, the remainder function ΔR must be considered, but then the evaluations become somewhat involved. If these evaluations are made, the maximum force and phase are again functions of the period parameter.

An alternative procedure is the direct establishment of the maximum force and phase by merely taking these quantities from the reduced force curves of this investigation. Such readings for the cylinders are given in figure 31 and for the plates in figure 32.

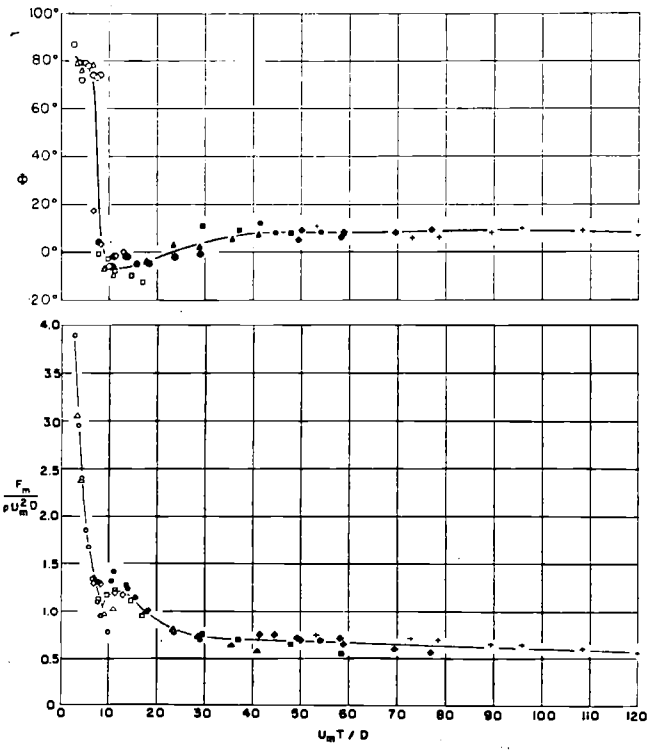

FIGURE 31. *Variations of the magnitude and phase of the maximum force on cylinders.*

Diameter (inches): 3 2.5 2 1.75 1.5 1.25 1 0.75 0.5
Corresponding symbol: ○ △ □ ◇ ● ▲ ■ ◆ +

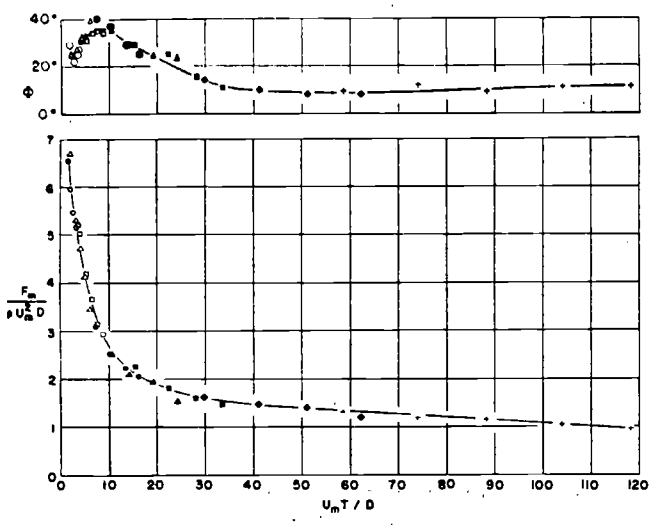

FIGURE 32. *Variations of the magnitude and phase of the maximum force on plates.*

Diameter (inches): 3 2.5 2 1.5 1.25 1 0.75 0.5
Corresponding symbol: ○ △ □ ● ▲ ■ ◆ +

TABLE 7. *Cylinders*

U_mT/D	$\frac{F_m}{\rho U_m^2 D}$	Φ (degrees)	U_mT/D	$\frac{F_m}{\rho U_m^2 D}$	Φ (degrees)
2.5	4.00	82.0	12.5	1.28	−6.8
3.0	3.45	81.2	15.0	1.15	−6.0
3.5	3.02	80.8	17.5	1.03	−5.0
4.0	2.65	80.0	20.0	0.93	−3.0
4.5	2.34	79.0	25.0	.80	1.0
5.0	2.10	78.0	30.0	.73	4.0
5.5	1.83	76.6	35.0	.70	6.5
6.0	1.60	75.0	40.0	.68	8.0
6.5	1.42	72.5	50.0	.66	8.0
7.0	1.30	65.0	60.0	.65	8.0
7.5	1.20	35.0	70.0	.63	8.3
8.0	1.20	5.0	80.0	.63	8.7
9.0	1.25	−3.0	90.0	.62	8.9
10.0	1.28	−6.0	100.0	.62	9.0

TABLE 8. *Plates*

U_mT/D	$\frac{F_m}{\rho U_m^2 D}$	Φ (degrees)	U_mT/D	$\frac{F_m}{\rho U_m^2 D}$	Φ (degrees)
2.0	6.50	24.0	10.0	2.71	34.9
2.5	6.00	25.6	12.5	2.44	32.0
3.0	5.55	27.0	15.0	2.25	28.5
3.5	5.20	28.2	17.5	2.10	26.0
4.0	4.85	29.5	20.0	1.96	23.5
4.5	4.55	30.8	25.0	1.76	18.3
5.0	4.30	32.0	30.0	1.63	13.6
5.5	4.05	33.0	35.0	1.53	11.1
6.0	3.82	33.6	40.0	1.45	9.7
7.0	3.43	34.9	50.0	1.33	8.9
8.0	3.10	35.5	60.0	1.25	8.7
9.0	2.86	35.5	70.0	1.18	9.0
--------	--------	--------	80.0	1.11	9.5
--------	--------	--------	90.0	1.06	10.1
--------	--------	--------	100.0	1.02	10.8

WASHINGTON, December 2, 1957.

For reference purposes, the data of the curves is given in tables 7 and 8, and can be used directly. In a future communication the forces on cylinders held in vertical positions will be computed on the basis of the data in these tables and will be compared with the laboratory observations already completed as a matter of concrete illustration.

The authors gratefully acknowledge the suggestions of G. B. Schubauer, the valuable and extensive endeavors of J. W. Lowry, a former colleague, in carefully examining the force records and preparing the corresponding charts and the diligence and resourcefulness of Victor Brame in carrying out the experiments.

11. References

[1] G. G. Stokes, On the effect of the internal friction of fluids on the motion of pendulums, Trans. Cambridge Phil. Soc. **9,** 8 (1851). (eq (51)).
[2] J. Boussinesq, Sur la résistance . . . d'une sphère solide . . . Compt. rend. **100,** 935 (1885).
[3] A. B. Basset, On the motion of a sphere in a viscous liquid Phil. Trans. Roy. Soc. London **179,** 43 (1888).
[4] Lord Rayleigh, On the motion of solid bodies through viscous liquid Phil. Mag. [6] **21,** 687 (1911).
[5] J. S. McNown and L. W. Wolf, Resistance to unsteady flow: I. Analysis of tests with flat plate, Engineering Research Institute, The University of Michigan, 2446-I-P, June 1956. Internal report to Sandia Corporation.
[6] J. R. Morison, M. P. O'Brien, J. W. Johnson, and S. A. Schaaf, The forces exerted by surface waves on piles, J. Petrol. Technol. Am. Inst. Mining Engrs. **189,** 149 (1950).
[7] J. R. Morison, J. W. Johnson, and M. P. O'Brien, Experimental studies of forces on piles. Coastal Engineering, Proc. Fourth Conference (1953).
[8] H. W. Iverson and R. Balent, A correlating modulus for fluid resistance in accelerated motion, J. Appl. Phy. **22,** 324 (1951).
[9] S. R. Keim, Fluid resistance to cylinders in accelerated motion. J. of Hydraulics Div., Proc. Am. Soc. Civil Engrs. **82,** Paper 1113 (1956).
[10] G. Bugliarello, The resistance to accelerated motion of spheres in water, Ricerca Sci. **26,** 437 (1956).
[11] R. O. Reid and C. L. Bretschneider, The design wave in deep water or shallow water, storm tide, and forces on vertical piling and large submerged objects. A. and M. College of Texas, Dept. of Oceanography, Tech. Report on Contract NOy-27474, DA-49-005-eng-18, and N7onr-48704, 36 pp., Feb. 1954 (unpublished).
[12] R. O. Reid, Analysis of wave force experiments at Caplen, Texas (Sun Oil Company platform). A. and M. College of Texas, Dept. of Oceanography, Tech. Report on Contract NOy-27474, 49 pp., January 1956 (Unpublished).
[13] F. D. Mornaghan, Bul. Natl. Research Council **84,** 46 (Washington, D. C., 1932).
[14] Sir Horace Lamb, Hydrodynamics, Sixth Ed., p. 77, Dover Publications.
[15] J. S. McNown, Drag in steady flow, The university of Michigan and Sandia Corporation, Proc. Intern. Congress Appl. Mech. Brussells (1957).
[16] R. Miche, Mouvements ondulatoires de la mer en profondeur constante ou décroissante, Ann. Ponts et Chaussées **114,** 25 (1944).
[17] M. P. O'Brien and J. R. Morison, The forces exerted by waves on objects. Trans. Am. Geophys. Union **33,** 33 (1952).
[18] J. S. McNown and G. H. Keulegan, Vortex formation and resistance in periodic motion (publication pending).